Desalination and Water Treatment
www.deswater.com
doi: 10.5004/dwt.2022.28711

268 (2022) 67–88
August

Evaluating the electrokinetic behavior of the acrylonitrile based Zn(II) ion-imprinted cross-linked polymer adsorbent for the Zn(II) ions selective removal from aqueous medium

Tanveer ul Haq Zia[a,*], Muhammad Hassaan Qureshi[a], Behisht Ara[b], Kashif Gul[b], Daud Khan Ghazali[a]

[a]*Department of Chemistry, Sarhad University of Science and IT, Landi Akhun Ahmad, Hayatabad Link Ring road, Peshawar (Khyber Pakhtunkhwa), 25000 Pakistan, Tel. +92-334 9011757; emails: tanveerics@gmail.com (T.U.H. Zia), mhq2310@gmail.com (M.H. Qureshi), duadtoofaan@gmail.com (D.K. Ghazali)*
[b]*Institute of Chemical Sciences, University of Peshawar, Jamrud road, Peshawar (Khyber Pakhtunkhwa), 25000 Pakistan, emails: bahishtara@gmail.com (B. Ara), kashifpkh@yahoo.com (K. Gul)*

Received 17 July 2021; Accepted 6 July 2022

ABSTRACT

Zn(II) ion-imprinted polymer [Zn(II) IIP] was prepared by following precipitation polymerization using acrylonitrile as functional monomer, N,N′-Methylenebis(acrylamide) as cross-linker and potassium persulfate as thermal initiator. Furthermore, 8-hydroxyquinoline was used as complexing agent for Zn(II) ions that was also employed for functionalizing the Zn(II) IIP. After the leaching of the Zn(II) ions, an ion-imprinted polymer [Zn(II) IIP] was obtained which showed high tendency of selective recombination with the Zn(II) ions. The equilibrium and kinetic adsorption studies of Zn(II) ions on both Zn(II) IIP and non-imprinted polymer (NIP) were carried out at different temperatures. Scanning electron microscopy and Fourier-transform infrared spectroscopy was carried out for evaluating the morphology and the various functional groups present in the molecular structure. The specific surface area was determined to be 337.30 $m^2\ g^{-1}$ for NIP whereas 439.54 $m^2\ g^{-1}$ for Zn(II) IIP by applying the Brunauer–Emmett–Teller model to the nitrogen adsorption isotherm. Similarly, the pore-size distribution was analyzed using the Barrett–Joyner–Halenda model and *t*-plot method confirming the surface texture of both adsorbent to be mesoporous in nature. The isotherm models of Langmuir, Freundlich, and Dubinin–Radushkevich were used to analyze the adsorption equilibrium data. It was revealed that the adsorbents surface has heterogeneous nature as Freundlich isotherm was more closely followed by the adsorbents. The maximum adsorption capacity was found to be 3.75 mg g^{-1} for NIP whereas 6.82 mg g^{-1} for Zn(II) IIP. The relative selectivity coefficient *K′* for Zn(II)/Co(II), Zn(II)/Cu(II), Zn(II)/Ni(II) and Zn(II)/Pb(II) metal ion pairs is determined to be 24.827, 1.273, 3.931 and 2.437, respectively. The adsorption kinetic data followed pseudo-first-order model with respect to R^2 values suggesting physical nature of adsorption. Electrokinetic study was also performed for understanding the nature of interaction between adsorbate and adsorbent which was validated on the basis of Grahame and pK-1 model depicting the surface electrostatic potential nature of charges. Van't Hoff plot was employed on the thermodynamic data of adsorption for attaining the change in entropy (ΔS) and enthalpy (ΔH), in addition to the Gibb's free (ΔG) change as well.

Keywords: Zn(II) ions; Ion-imprinted polymer; Brunauer–Emmett–Teller; Acrylonitrile; Freundlich; Cross-linked polymer; Relative selectivity coefficient; pK-1 model

* Corresponding author.

1. Introduction

For human health, among the trace elements essential in diet for development and growth, zinc occupy an important position as it is a known fact that zinc deficiency in the nutrition of humans could lead to serious health issues and biological abnormalities such as intrauterine growth restriction, late sexual maturity, and reduced adaptive immunity. Zinc is potent to cell physiology such as various biological functions including cell metabolism, cell division, DNA translation for protein biosynthesis and plays an important role in membrane-stabilizing along with the antioxidant activity and sustains sperm period of validity by DNases inhibition [1]. A number of metalloenzymes use Zn(II) as structural and catalytic cofactor such as RNA polymerases that helps in gene regulation and DNA replication, superoxide dismutase compromising cell's frontline against the reactive oxygen species (ROS), and carbonic anhydrase habituating enzymatic functions of erythroid cells, the renal collecting tubules, gastric delomorphous cells and muscle tissue [2]. Moreover, zinc is involved in the synthesis and the breakdown of carbohydrates, lipids, proteins and nucleic acids, and in the metabolism of other trace elements [3]. On the other hand, presence of excess amount of zinc in human body could also result in various adverse health problems such as the electrolyte imbalance, nausea, anaemia and lethargy [4]. Therefore, there is dire need for the selective adsorbents in order to separate and pre-concentrate trace amount of zinc in complex matrix such as environmental, food, pharmacological and biochemical samples using facile and sensitive method of analysis. In addition, the removal of excess zinc during water treatment process is also an important area that requires further consideration.

Different solid sorbents have been applied previously for solid phase extraction of Zn(II) from various matrices. Kolev et al. [5] used polymer inclusion membrane (PIM) which was functionalized by immobilizing di(2-ethylhexyl)phosphoric acid (D2EHPA) as metal ion carrier onto poly(vinyl chloride) (PVC) to be used as Zn(II) selective solid phase for purpose of extraction in the presence of interfering agents such as Cd(II), Co(II), Cu(II), Ni(II) and Fe(II) in aqueous medium. Similarly, multi-walled carbon nanotubes (MWCNTs) functionalized with metal ion carriers such as di-(2-ethylhexyl)phosphoric acid (D2EHPA) and tri-n-octyl phosphine oxide (TOPO) has been applied as solid phase adsorbent for Zn(II) ions in natural water samples with an enrichment factor of 25, adsorption capacity of 4.82 mg g^{-1} and detection limit of 60 μg L^{-1} [6]. Amino groups were immobilized on silica gel which were chemically functionalized with p-dimethylaminobenzaldehyde (p-DMABD) and used as a selective adsorbent for Zn(II) solid phase extraction using batch and column methods as reported by Chang et al. [7]. Inductively coupled plasma-optical emission spectrometry (ICP-OES) was applied as a technique for metal ions determination. Zhao et al. [8] synthesized Zn(II) ion-imprinted polymer using 8-acryloyloxyquinoline (8-AOQ) monomer and ethylene glycol dimethacrylate (EGDMA) as a cross-linker while applying 2,2′-azobisisobutyronitrile (AIBN) as thermal initiator. Leaching was performed to remove Zn(II) ions from the cross-linked co-polymer which resulted in selective adsorbent for Zn(II) ion solid phase extraction showing maximum adsorption capacity of 3.9 mg g^{-1}. The cross-linked co-polymer of acrylonitrile with N,N′-Methylenebis(acrylamide) was modified with 2-aminopyridine and used as an adsorbent for Hg(II), Cd(II) and Cr(III) ion showing an adsorption capacity of 3.3, 0.94 and 0.43 mmol g^{-1}, respectively [9]. The use of novel polymers for ion imprinting intended for heavy metals separation has attracted considerable attention such as the latest studies highlights its background for its potential design and synthesis for the elaboration of the adsorption mechanism [10,11].

Ion-imprinted polymers (IIPs) are functionalized polymeric adsorbents that are selective in nature to specific analyte for which it is designed which renders them suitable for either metal ions removal or pre-concentration when it comes to handling of the complex matrix [12]. As for an analytical process, sample preparation is of significant importance as inappropriate pretreatment of sample will result in loss of target analyte as well as its contamination that can compromise the accuracy of data of the research [13]. Similarly, the target analyte enrichment and their isolation from matrices of complex nature is also a prime challenge when performing analytical measurements [14]. The fundamental aspect of ion imprinting adsorbent is the metal ion's binding affinity with the active site which is the consequence of the metal ion complexation with the chelate. The ability of the ion-imprinted polymers (IIPs) is to recognise ion selectively which can be used under severe conditions of high acidity or alkalinity, high temperature and pressure in addition to their facile and low cost preparation [15]. The first step in the ion imprinting process is the preparation of metal ion complex with a suitable ligand followed by its entrapment in the cross linked polymer matrix and finally the removal of the metal ion (template) to leave behind an active recognising site which will be able to selectively distinguish between the template and other interfering metal ions in the matrix. The ion-imprinted polymers can have various dimensions having specific binding sites for template in the form of particle (nano/micro), beads, monolith, cryogel or hydrogel [16]. These selective polymeric adsorbents can be utilized to prepare packed columns that have required selectivity level [17].

Flame atomic absorption spectrometry (FAAS) is an analytical technique that has significant importance when it comes to metals determination at trace amounts of parts per million (ppm) and parts per billion (ppb) along with sensitivity and selectivity [18,19]. The sensitivity of FAAS can further be improved when the matrix containing metal is subjected to separation and pre-concentration treatment using a selective adsorbent such as ion-imprinted polymers (IIPs) which has chemical affinity for the target metal in the matrix. Factors such as the ligand-metal interaction, metal ion complex symmetry, metal ion charge and coordination number and interactive electrostatic affinity between the cross-linked polymer and metal ion complex determine the selectivity and sensitivity of IIPs [20]. Therefore, ion-imprinted polymers (IIPs) received considerable attention in the field of research for application in catalysis,

chromatography, solid-phase extraction, supported liquid membrane extraction and sensors [21].

For the present study, a Zn(II) ion-imprinted polymer was prepared by precipitation polymerization using potassium persulfate as thermal initiator, with the focus on the selective recognition of Zn(II) ions. The metal complex was prepared by using 8-hydroxyquinoline as complexing agent for Zn(II) ions. The metal complex was then entrapped physically as a template for Zn(II) ions, in the cross-linked polymer of acrylonitrile as functional monomer and N,N′-Methylenebis(acrylamide) as cross-linker. After the removal of Zn(II) ions from cross-linked polymer leaving behind active sites, resulted in a highly selective imprinted solid phase which was used to pre-concentrate and determine Zn(II) ions concentration in target matrix by flame atomic absorption spectrometry (AAS).

2. Materials and methods

2.1. Materials

Acrylonitrile which was stabilized with hydroquinone monomethyl ether was used as a functional monomer for synthesis and was purchased from Sigma-Aldrich (Merck). N,N′-Methylenebis(acrylamide) with 99% purity was used as cross-linker and was purchased from Sigma-Aldrich (Merck). Deionized water was used as solvent and potassium persulfate (99% purity) as thermal initiator was also purchased from Sigma-Aldrich (Merck). 8-hydroxyquinoline having 99% purity was purchased from Sigma-Aldrich (Merck) and used as a chelating agent for Zn(II) ions. Zinc sulfate heptahydrate ($ZnSO_4 \cdot 7H_2O$) was also procured from Sigma-Aldrich (Merck) having 99% purity. For the purpose of performing leaching, glacial acetic acid (99.7%) was procured from Alfa Aesar (Thermo Fisher Scientific). Commercial methanol was purchased which was double distilled prior to use.

2.2. Instrumentation

For the purpose of metal determination, flame atomic absorption spectrophotometer purchased from Perkin-Elmer, USA (AAnalyst 800) was used which applied deuterium background correction while having CTA 2000 as single-element hollow cathode lamp and Zn(II) absorbance was recorded at 213.9 nm applying a spectral bandwidth of 0.5 nm. For observing the morphology of the cross-linked polymeric adsorbents, scanning electron microscopy (SEM) micrographs were captured using a JEOL JSM-6300 (Japan) for which the aqueous solutions of the cross-linked polymeric adsorbents were dried on a glass slide under vacuum for approximately 4 h at 60°C and subsequently, sputter coated with gold. PerkinElmer Spectrum 1000 (USA) Fourier-transform infrared (FTIR) spectrophotometer, having 1 cm^{-1} resolution, was applied to record the infrared (IR) transmittance spectra using KBr pellet at room temperature. For minimizing the solvent molecules interference in FTIR spectrum, the cross-linked polymeric adsorbents were placed under vacuum for drying at 60°C for 2 h. For measuring the specific surface area along with the porosity and pore-size distribution of the cross-linked polymeric adsorbents, N_2 adsorption was performed at liquid nitrogen temperature (77.350 K) using the Quantachrome NOVA 2200E model. In order to remove adsorbed gases (N_2,O_2) and moisture from the samples, they were placed under high vacuum for heating at 70°C for 6 h in a vacuum oven prior to analysis. For determining the parameters of the electrokinetic, the electrostatic (zeta) ξ-potential was measured at 25°C by applying a Malvern Zetasizer Nano ZS (UK) that utilizes a laser (4 mW He–Ne laser at λ_{max} = 633 nm) Doppler electrophoresis technique using the folded capillary cell equipped with the electrodes of gold. Zetasizer software was used to perform instrument calibration in order to minimize the noise which appears in the laser signal during data collection. A delay time of 5 min was set in order for the sample to equilibrate before carrying out the measurement of the electrophoretic mobility data which was used in the following equation to determine the electrostatic (zeta) ξ-potential [22];

$$\xi = \frac{3\eta U_E}{2\varepsilon(\kappa\alpha)} \tag{1}$$

where U_E is the electrophoretic mobility, ε is the medium permittivity constant, η is medium's viscosity, 1/κ denotes the Debye length which is the statistically calculated electrical double layer thickness of ions present at the surface, α is the radius of the particle and $f(\kappa\alpha)$ represents the Henry's function value, determined while assuming 1.5 value for Smoluchowski approximation on the basis of Smoluchowski model, for aqueous medium which is polar having moderate electrolyte concentration [23]. Furthermore, in order to evaluate adsorbent's pH_{pzc} that represents the pH at which point of zero charge is acquired, a colloidal suspension having 0.1 g L^{-1} adsorbent is prepared in the deionized water which was ultrasonicated for 40 min to acquire maximum pH relaxation that is controlled by using 10^{-2} N aqueous solutions of NaOH and HCl. After obtaining the supernatant liquid from the sample followed by centrifugation, was used for the electrostatic ξ-potential measurement.

2.3. Non-imprinted polymer synthesis

Non-imprinted polymer was synthesized by adding 12 mL deionized water in a vial as a solvent, 0.96 g acrylonitrile as a functional monomer, 0.1 g N,N′-Methylenebis(acrylamide) as a cross-linker and 0.2 g potassium per sulfate was taken as an initiator followed by heating at 90°C for 3 h in water bath. The proceeding of the reaction was followed by observing the appearance of white precipitates in reaction mixture. Washing was performed through centrifugation where deionized water and methanol was used to wash the non-imprinted polymer and was kept in oven for drying at 100°C for 24 h. Afterwards, the samples were crushed to powder in agate mortar and pestle.

2.4. Zn(II) ion-imprinted polymer [Zn(II) IIP] synthesis

The Zn(II) IIP synthesis is depicted in Fig. 1. Zn(II) complex was formed using 8-hydroxyquinoline as a chelating

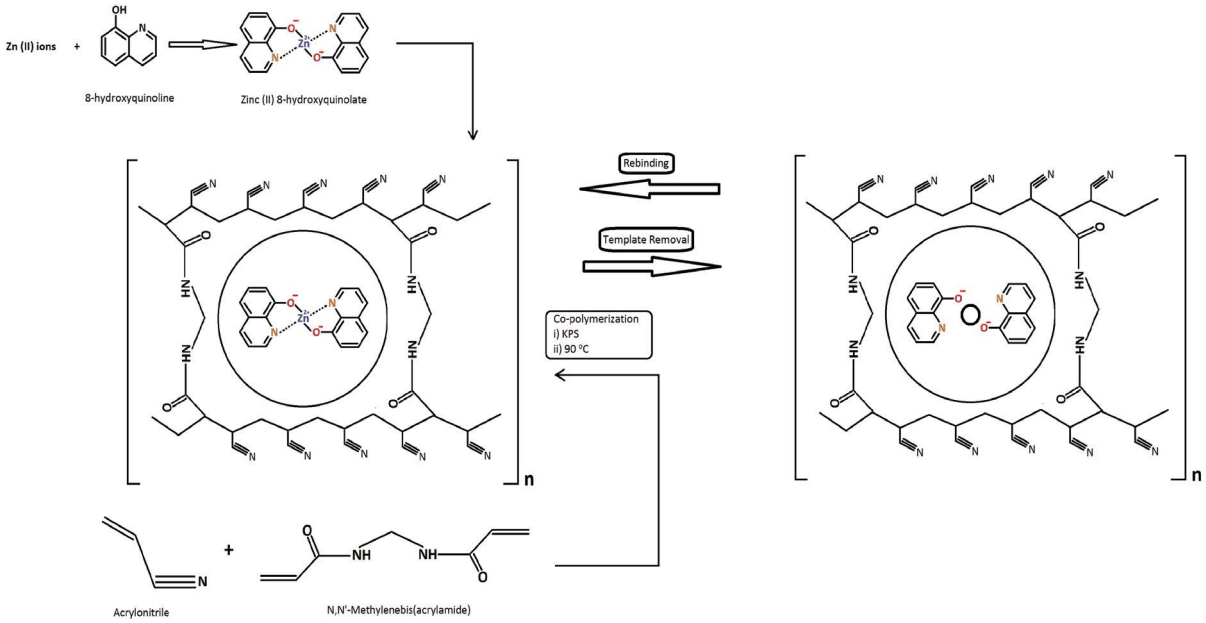

Fig. 1. Preparation of ion-imprinted polymer (IIP) [Zn(II) IIP].

agent at pH-10 by adding 3 mL of 100 mg L^{-1} of $ZnSO_4{\cdot}7H_2O$ salt aqueous solution, 7 mL of 100 ppm of 8-hydroxyquinoline and 2 mL pH-10 in a vial. After complex formation polymer reagents were added in the following sequence, 0.96 g acrylonitrile as a functional monomer followed by 0.1 g N,N′-Methylenebis(acrylamide) as a cross-linker and 0.2 g potassium per sulfate as an initiator. The vial was heated at 90°C for 3 h in water bath and the proceedings or the polymer reaction was followed by observing the white precipitates in the reaction mixture. Zn(II) IIP was washed with methanol to remove unreacted reagents and then washed with 56% acetic acid and 1M HCl solutions to remove the template ion. Drying was performed in oven at 100°C for 24 h. Afterwards, the samples were crushed to powder in agate mortar and pestle.

2.5. Determination of surface charge

In order to determine the surface charge density as function of pH, acid–base potentiometric titrations were carried out with constant background electrolyte concentration. The respective H^+ and OH^- ions adsorption densities, determined using the surface area S of the adsorbents and the initial and final pH after adsorbent was added to the known amount of acid or base in a suspension, were used to determine the surface charge density σ^M as [24,25];

$$\sigma^M = F\left(\Gamma_{H^+} + \Gamma_{H^-}\right) \tag{2}$$

$$\Gamma_{H^+} = \frac{\left(n_{H^+} - n^b_{H^+}\right)}{S} \tag{3}$$

$$\Gamma_{OH^-} = \frac{\left(n_{OH^-} - n^b_{OH^-}\right)}{S} \tag{4}$$

where F denotes the Faraday's constant, Γ_{H+} & Γ_{OH^-} are the H^+ and OH^- ions number of moles adsorbed per cm^2, n_{H^+} and n_{OH^-} are the total H^+ and OH^- ions number of moles added to the suspension, $n^b_{H^+}$ and $n^b_{OH^-}$ are the number of moles added to blank to give the same pH. A constant background electrolyte concentration 0.01 N KCl was employed to fix the activity coefficient during the titrations. For performing the acid–base titration, standardized aqueous solutions of HNO_3 (0.1 M) and KOH (0.1 M) were used for attaining the required pH either on the acidic or basic side. In the same way, blank titrations were carried out in the absence of the adsorbents.

2.6. Equilibrium binding experiment

Batch equilibrium binding experiments were performed to study the adsorption isotherms, thermodynamic and kinetics parameters [26]. To perform this experiment, 0.05 g cross-linked polymeric adsorbent was added to 5 mL solution of adsorbate at neutral pH. In order to achieve dynamic equilibrium for adsorption of adsorbate on adsorbent, orbital shaker (MaxQ7000) with thermostatic water bath was applied for shaking purpose for 5 h at 100 rpm as shaking speed. The adsorbents were separated through centrifugation (Hettich MIKRO 220) from the adsorbate solution when performed for 30 min at 10,000 rpm followed by determining adsorbate concentration in the supernatant by employing a flame atomic absorption spectrophotometer [27]. The adsorption equilibrium and thermodynamic data was determined for adsorption of Zn(II) on both the non-imprinted polymer (NIP) as well as Zn(II) IIP at four different temperatures (303, 323, 343, and 363 K) using Zn(II) solution with different concentration in the range of 20 to 100 mg L^{-1}.

2.7. Kinetic study

Kinetic study of Zn(II) ions adsorption on both NIP as well as Zn(II) IIP was found at four different temperatures (303, 323, 343, and 363 K) by adding 0.05 g of each adsorbent separately in the 5 mL of 100 mg L^{-1} of Zn(II) solution for different time interval. Variations in the time were 10, 30, 60, 120 and 180 min respectively. Both NIP as well as Zn(II) IIP was separated from the solution via centrifugation and the flame atomic absorption spectrophotometry was performed to find the equilibrium concentration of Zn(II) in supernatant solution. The data was further analysed by using the important kinetic models known as pseudo-first-order, pseudo-second-order and intraparticle diffusion model.

2.8. Selectivity studies

For evaluating the imprinted polymer's selectivity, competitive adsorption was carried out for the Zn(II) ions and other metal ions (M) on NIP and Zn(II) IIP as adsorbents by employing their mixtures, respectively. The expressions for the K_d (mL g^{-1}) denoting distribution coefficient, k representing the selectivity coefficient, and the k' as relative selectivity coefficient are given below as:

$$K_d = \frac{\left(C_o - C_e\right)V}{C_e m} \tag{5}$$

$$K_d = \frac{K_{d\ \mathrm{Zn(II)}}}{k_{d(M)}} \tag{6}$$

$$k' - \frac{k_{(\mathrm{IIP})}}{k_{(\mathrm{NIP})}} \tag{7}$$

where C_o and C_e denotes the initial and equilibrium concentration of the each respective metal ion in solution. $K_{d\ \mathrm{Zn(II)}}$ and $K_{d\ \mathrm{(M)}}$ denotes Zn(II) and M ions distribution coefficient, respectively. Similarly, Zn(II) and M ions selectivity coefficient are $k_{(\mathrm{IIP})}$ and $k_{(\mathrm{NIP})}$, respectively (M denotes the interfering metal ion).

3. Results and discussion

3.1. Scanning electron microscopy

For observing the morphology of NIP and Zn(II) IIP adsorbents, micrographs were taken using SEM. The NIP adsorbent show homogeneity with respect to shape having nearly oblate spheroid shape beads with narrow size distribution with homogeneous dispersion ranging from 100 to 300 nm in diameter as shown in Fig. 2a. Whereas the SEM micrographs of the Zn(II) IIP adsorbent show wide size distribution with range from 70 to 250 nm in diameter and also show minor agglomeration and non-uniform polydispersity. In addition, the Zn(II) IIP adsorbent appear to have more rough topological appearance than NIP adsorbent which indicates imprinted cavities formation at surface leading to increase in porosity and hence the specific surface also increase which is the reason of increase in the adsorption surface phenomenon as shown in Fig. 2b that also depicts the interaction between the polymer and metal ion complex.

3.2. Fourier-transform infrared spectroscopy

There is similarity in the backbone of the co-polymer comprising of acrylonitrile as monomer and N,N'-Methylenebis(acrylamide) as a cross-linker in NIP and Zn(II) IIP cross-linked polymeric adsorbent due to which the molecular structures for both bears similarity in the IR spectrum as shown in Fig. 3. The characteristic IR peak for amide (N–H) group stretching vibrations appears at 3,350 cm^{-1} whereas the stretching vibrations of carbonyl (C=O) group for secondary amide show strong absorption peak at 1,672 cm^{-1} and weak IR peak at 2,244 cm^{-1} can be assigned to nitrile (C≡N) group stretching oscillations [28]. The N–H bending vibration has peak that appears at 1,526 cm^{-1} [29]. For the Zn(II) ion-imprinted polymer, the characteristics IR peak at 785 cm^{-1} is assigned

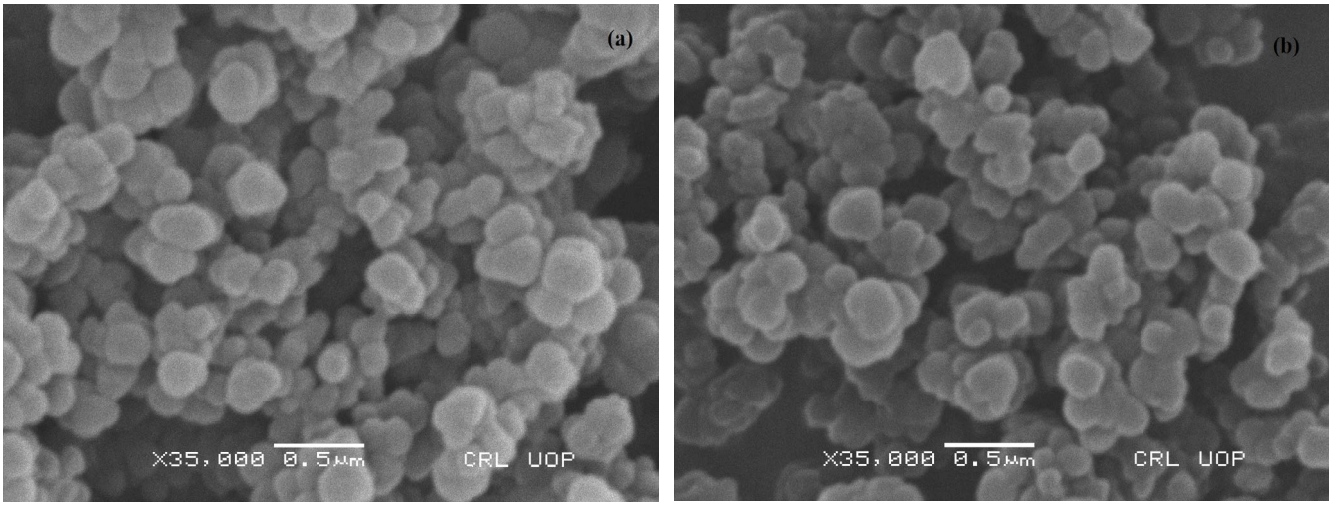

Fig. 2. SEM micrographs of (a) non-imprinted (NIP) polymer and (b) Zn(II) ion-imprinted (IIP) polymer adsorbents.

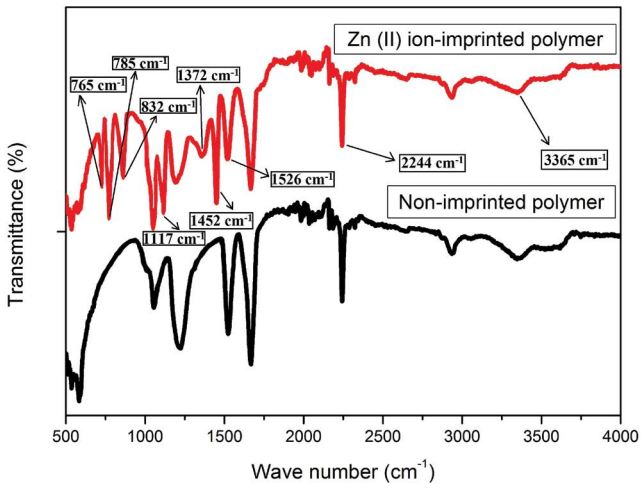

Fig. 3. FTIR spectrum of non-imprinted (NIP) and Zn(II) ion-imprinted (IIP) polymer.

to C–H wagging mode of vibration attributed to presence of 8-hydroxyquinoline coordinated to Zn(II) cation. The absorption peaks at 732 and 824 cm^{-1} (C–H wagging) ascribed to Zn(II) cation complex with 8-hydroxyquinoline as reportedly previously, show slight shift to higher frequencies at 765 and 832 cm^{-1} which can be attributed to the formation of coordination complex between Zn(II) ion and at 8-hydroxyquinoline [30,31]. The strong absorption peak at 1,117 cm^{-1} can be attributed to C–O stretching vibrations at the C–O–M site [32]. The peaks associated with aromatic ring stretching in 8-hydroxyquinoline appear at 1,372 and 1,452 cm^{-1}. The absence of IR peak at 1,630 cm^{-1} attributed to double bond stretching vibrations confirms the absence of the reactive vinyl group [29].

3.3. Surface area analysis

The capillary condensation is prime mechanism behind the stepwise accumulation of the adsorbate at the porous surface which can be termed as pore filling phenomenon as depicted in the nitrogen adsorption isotherms of NIP and Zn(II) IIP adsorbents as shown in Figs. 4 and 5. The multilayer model of Brunauer–Emmett–Teller (BET) adsorption isotherm is fitted linearly below the recommended p/p^o limit on the equilibrium adsorption data for N_2 adsorption at the adsorbent surface leading to the multilayer formation, for evaluating the adsorbent's specific surface area;

$$\frac{1}{\left[Q\left(\frac{p^o}{p}-1\right)\right]}=\frac{c-1}{Q_m c}\left(\frac{p}{p^o}\right)+\frac{1}{Q_m c} \tag{8}$$

where Q is the volume of adsorbed gas per unit adsorbent mass ($cm^3\ g^{-1}$), Q_m is the volume of adsorbed gas when surface coverage is unimolecular ($cm^3\ g^{-1}$), p^o is the standard pressure, p is the equilibrium pressure and c is the constant which relates the heat of adsorption to heat of liquefaction at constant temperature [33]. For NIP adsorbent, the evaluated BET specific surface area is found to be 337.30 $m^2\ g^{-1}$ whereas 439.54 $m^2\ g^{-1}$ specific surface area is observed for Zn(II) IIP adsorbent and this prominent increment can be attributed to the formation of imprinting cavities at the surface and in the bulk leading to an increase in the number of active sites.

In order to evaluate statistically the thickness of adsorbate at the adsorbent surface, de-Boer equation is applied which is given as;

$$t\left(\dot{A}\right)=\left(\frac{13.99}{\log\left(\frac{p^o}{p}\right)+0.034}\right)^{1/2} \tag{9}$$

where t represents the adsorbed layer statistical thickness ($\dot{A}$) [34]. By plotting the quantity of N_2 gas adsorbed per gram of adsorbent at the relative pressure against the thickness t (P), t-plot is attained which provides an insight into the porous adsorbent surface through evaluating the pore internal as well as external surface coverage. When the adsorbent surface is non-porous, a linear t-plot is obtained. On the other hand, non-linear t-plot is obtained when the absorbent surface possesses porous texture. The total surface area incase of the porous texture can be attributed to both internal and external surface coverage and can be evaluated from the linear fitting of t-plot region before the capillary condensation occurrence. After the capillary condensation leading to pore internal surface coverage is achieved, is followed by the occurrence of adsorption on the external surface which can be obtained from the slope of the linear fit of the t-plot region corresponding to external adsorption whereas the intercept provides the value of the mesoporous volume. As these two regions are apparently visible in the t-plot, it points the fact that the adsorbents are mesoporous in nature. In case of NIP adsorbent, the mesopore volume is found to be 0.332 $cm^3\ g^{-1}$ which shows an increase to 0.364 $cm^3\ g^{-1}$ for Zn(II) IIP adsorbent. Similarly, the mesoporous surface area obtained by the subtraction of the external surface are from the total surface area is 183 $m^2\ g^{-1}$ for NIP adsorbent and 297 $m^2\ g^{-1}$ for the Zn(II) IIP adsorbent. When the linear fir in t-plot region of low pressure fails to pass through origin leads to false speculation of the microporosity presence as this method is suitable for evaluating the adsorption data if mesopores are 10 times in size as compared to the adsorbate molecule (N_2 molecule). Therefore, if the diameter of the mesopore is large, then it could be assumed that the mesoporous surface adsorption follows the mechanism of the flat surface adsorption [35].

The polydispersity in the pore size is apparent in the nitrogen adsorption isotherm as pore condensation phase is not prominent. So the pore size as well as pore-size distribution is evaluated by applying Barrett–Joyner–Halenda (BJH) method of analysis to the nitrogen adsorption isotherm for adsorption at 77 K when cylindrical pore shape is presumed (Area of pore $= A_p = \frac{2V_p}{r_p}$) for completely characterizing the surface texture and corresponding equations for measurements are given as [36];

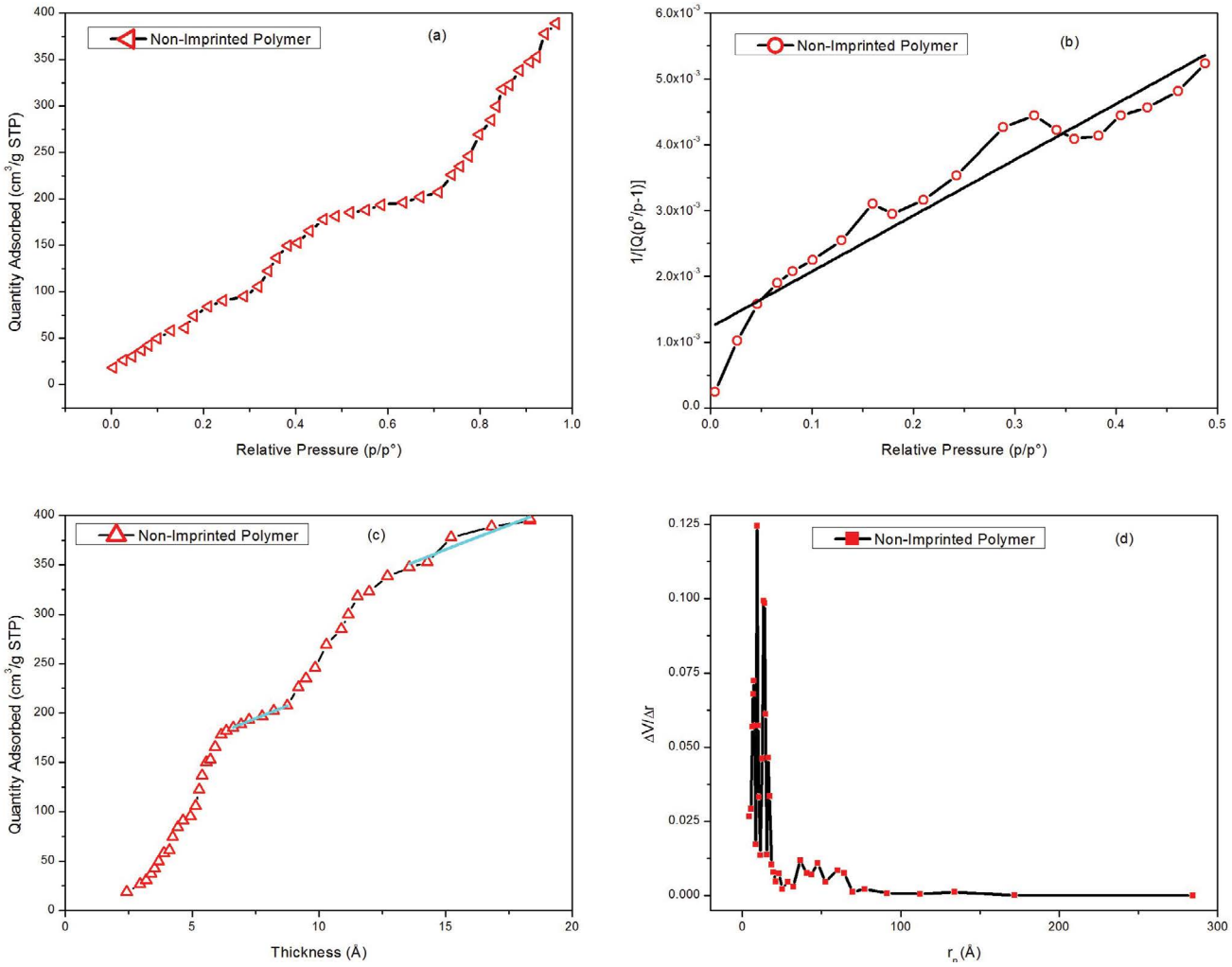

Fig. 4. (a) Nitrogen adsorption isotherm at 77 K, (b) BET surface area plot for nitrogen adsorption at 77 K with linear fitting, (b) *t*-plot model applied on nitrogen adsorption at 77 K with linear fitting, and (c) BJH model pore-size distribution for non-imprinted (NIP) polymer.

$$V_p = R_n \Delta V - R_n c \sum_{j=1}^{n-1} A_{pj} \tag{10}$$

$$R_n = \frac{r_p^2}{\left(r_k + \Delta t\right)^2} \tag{11}$$

$$c = \frac{\left(\overline{r}_p - t_r\right)}{\overline{r}_p} \tag{12}$$

$$\log \frac{p}{p^o} = \frac{-4.14}{r_k} \tag{13}$$

where pore volume is represented as V_p, given volume of gas desorbed is ΔV_p, radius of pore which is empty is given as r_p, radius of inner capillary of pore if physically adsorbed layer is present is denoted as r_k and the adsorbed layer statistical thickness is t_r. For NIP as well as Zn(II) IIP, the size of pore is greater than 6 nm confirming the presence of the mesoporosity in both the polymer adsorbents respectively. The remaining physical parameters of texture of surface as obtained by BET model and *t*-plot method are presented in Table 1.

3.4. Electrokinetic analysis

On the basis of the Gouy–Chapman theory, the approximation is performed using Boltzmann factor for the concentration of the ionic specie in close proximity of the charged surface in order to acquire the total charge available per unit volume ϱ(*x*) as;

$$\rho\left(x\right) = \sum_i n_i^o z_i e \exp\left(\frac{-z_i e \xi}{kT}\right) \tag{14}$$

where the concentration of ionic specie in the bulk is represented as n_i^o, the ionic specie valency is denoted as z_i, charge on the electron is given as e (C), k is the Boltzmann

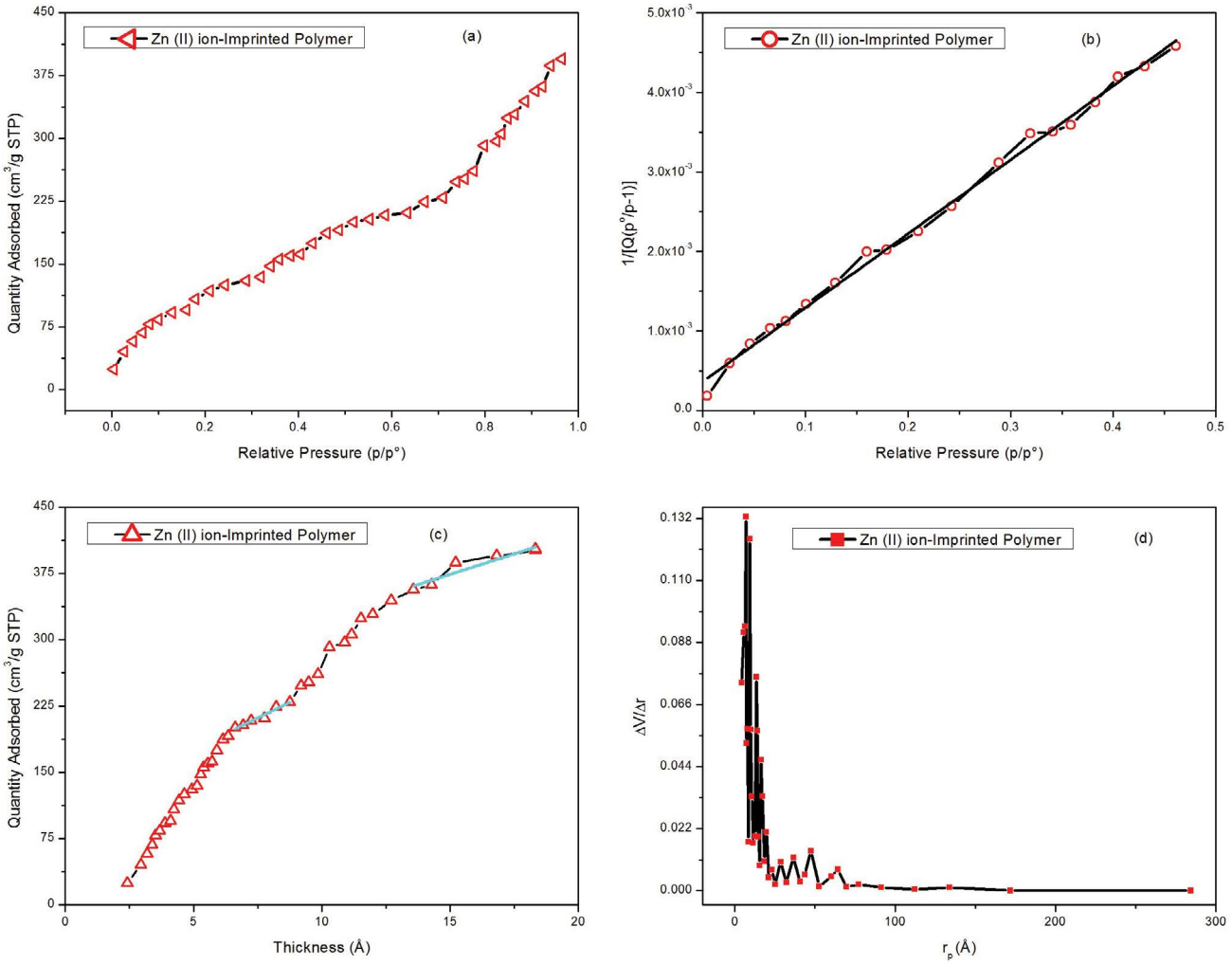

Fig. 5. (a) Nitrogen adsorption isotherm at 77 K, (b) BET surface area plot for nitrogen adsorption at 77 K with linear fitting, (c) *t*-plot model applied on nitrogen adsorption at 77 K with linear fitting, and (d) BJH model pore-size distribution for Zn(II) ion-imprinted (IIP) polymer.

Table 1
Typical textural and surface parameters derived from N_2 adsorption at 77 K on non-imprinted polymer (NIP) and Zn(II) ion-imprinted (IIP) polymer using BET and *t*-plot models

Adsorbents	BET adsorption isotherm model				*t*-plot method				
	S_{BET} ($m^2\ g^{-1}$)	c	Q_m	R^2	$V_{Mesopore}$ ($cm^3\ g^{-1}$)	$S_{Mesopore}$ ($m^2\ g^{-1}$)	$S_{External}$ ($m^2\ g^{-1}$)	$S_{t\text{-plot}}$ ($m^2\ g^{-1}$)	R^2
NIP	337.30	15.29	77.49	0.93	0.332	32.56	182.83	0.019	0.92
Zn(II) IIP	439.54	27.29	100.96	0.99	0.364	43.95	296.61	0.017	0.95

constant, zeta potential is represented as ξ (mV) and T is the absolute temperature (K) [37]. On the other side, for a symmetrical electrolyte, the Poisson Boltzmann expression is represented as;

$$\frac{d\xi}{dx} = \left(\frac{8kTn^{o}}{\varepsilon\varepsilon_{o}}\right)^{1/2} \sinh\left(\frac{ze\xi}{2kT}\right) \tag{15}$$

It is elaborative in the above expression that there is alteration in the ξ zeta potential with respect to the distance of the accumulated charge in the surface proximity occurring in the diffuse layer. As we know that the adsorbent surface charge density σ^M is approximately equal to solution phase charge density σ^S, therefore, the charge per unit area $\sigma^M = q/A$ on adsorbent surface is monotonically related to ξ potential as;

$$\sigma^M = -\sigma^S = \frac{q}{A} = \varepsilon\varepsilon_o\left(\frac{d\xi}{dx}\right) \tag{16}$$

$$\sigma^M = \left(8kT\varepsilon\varepsilon_o n^o\right)^{1/2}\sinh\left(\frac{ze\xi}{2kT}\right) \tag{17}$$

Eq. (17) also known as the Grahame equation carries the significance for satisfying the condition of electroneutrality as the charge in the double layer solution phase becomes equal to the surface charge and is shown in Fig. 6b [38]. Similarly, when the positive and negative sites at the surface of the adsorbent achieve equality, then the state of the point of zero charge (pzc) is attained at the adsorbent's surface referring to the zero surface charge density and is also represented as pH_{pzc} represented in Fig. 6a. When the pH value is below the pH_{pzc}, the adsorbent surface is abundant with the positive charged sites and for pH values above pH_{pzc}, it is predominantly populated with the negatively charge sites due to which there is a prominent effect of pH on the adsorbent's ξ potential as shown in Fig. 6a and b. The amino group in the acrylonitrile undergoes protonation to NH_3^+ group with the pH increase resulting an overall increment in the ξ potential values for both the non-imprinted as well as Zn(II) ion-imprinted polymer [39]. There is also the adsorption of the H^+ ions at the surface of adsorbent causing a shift in ξ potential to positive side. The Zn(II) IIP have higher ξ potential as compared to NIP because of the introduction of the additional functionalities due to presence of the 8-hydroxyquinoline which has the ability to gain or lose proton that either results in dissociation or formation of 8-hydroxyquinolinato-chelate complexes which can also be an associated reason for the ξ potential decrease with pH values increase as well [40]. As obvious in Fig. 6a, for NIP, the pH_{pzc} is 6.6 which reduce to 5.9 for Zn(II) IIP, respectively.

The electrokinetic properties of the polymer adsorbents depends upon the pH of a solution which is on contact with them as the surface molecular groups of adsorbents exposed to the surrounding environment show alteration in there ionic state corresponding to the pH change in the solution. Since the increase in the pH value increase the negative charge on the adsorbent surface due to which the positively charged Zn(II) ion forms complex with active sites on the surface of adsorbent due to attractive electrostatic forces resulting an increase in the adsorption efficiency as shown in Fig. 6c. On the other hand, the repulsive electrostatic forces are prominent between adsorbent and adsorbate at the pH value below pH_{pzc} [41].

It is assumed that either the surface moieties when undergo ionization or the charge determining ions when adsorb at the surface is responsible for the surface charge. The aqueous ions distribution in the surface vicinity is influenced by the surface charge leading to the formation of an electrical double layer. The surface charge density is given as [42];

$$\sigma^M = \frac{1}{2}N\left\{\left[\mathrm{SOH}_2^{\frac{1}{2}+}\right] - \left[\mathrm{SOH}^{\frac{1}{2}-}\right]\right\} \tag{18}$$

where the $SOH_2^{1/2+}$ (Γ_{H^+}) and $SOH^{1/2-}$ Γ_{OH^-} represents the surface groups in protonated and deprotonated states with concentration given in moles per litre denoted by square brackets '[]'. Similarly, N is the unit conversion factor for transforming the concentration units to the charge density units which is given as

$$N = \frac{FV}{AM} \tag{19}$$

where the Faradays constant is denoted as F, V is solution volume, A denotes the specific surface area and M is the mass of the adsorbent. Since the Gouy–Chapman theory is the basis of Eq. (17), which is known as Grahame equation that correlates the surface charge density σ^M to the observed zeta potential ξ value while taking into consideration the diffuse layer that validates it for the background electrolyte which is symmetric 1:1. The high values of the zeta potential ξ do correspond to the high surface charge density that plays key role not only in stabilizing the colloidal dispersion but also facilitates the adsorption process. As evident in Fig. 6d and e, the theoretically determined values does follow the empirical values which depicts the fact that surface groups on both the NIP as well as Zn(II) IIP show the pK-1 model behavior in protonation and deprotonation [43].

3.5. Adsorption equilibrium studies

While keeping in view that the adsorption equilibrium is achieved in 90 min, and then for calculating the adsorption efficiency, the following expression is adopted [44];

$$\text{Adsorption Efficiency} = \frac{C_o - C_e}{C_o} \times 100 \tag{20}$$

where the initial concentration is denoted as C_o while C_e represents the equilibrium concentration of adsorbate dye (mg L^{-1}). The adsorption efficiency for the adsorption of Zn(II) ions on both Zn(II) IIP and NIP adsorbent was found at four different temperatures (298, 323, 343, and 363 K) which was plotted as the adsorption efficiency against the initial adsorbate concentration. As shown in Fig. 7a, that in case of NIP adsorbent, there was availability of active sites for adsorption at the beginning of the adsorption phenomenon due to which adsorption efficiency showed a raise at low initial adsorbate concentration. But as the concentration increased from 40 to 100 mg L^{-1}, a decrease was observed in the adsorption efficiency which was the indication of the decrement in available active sites. It could also be stated that when once the equilibrium was established, then no more active sites were available for adsorption of Zn(II) ions. Similar explanation can be given for adsorption of Zn(II) ions on the Zn(II) IIP as shown in Fig. 7b, but the adsorption efficiency was greater as compared to NIP as there were more active sites at the surface due to imprinting using 8-hydroxyquinoline as chelating agent which served as an incremental factor for increase in adsorption of Zn(II) ions [45]. However, it was observed that with the elevation in temperature, the adsorption

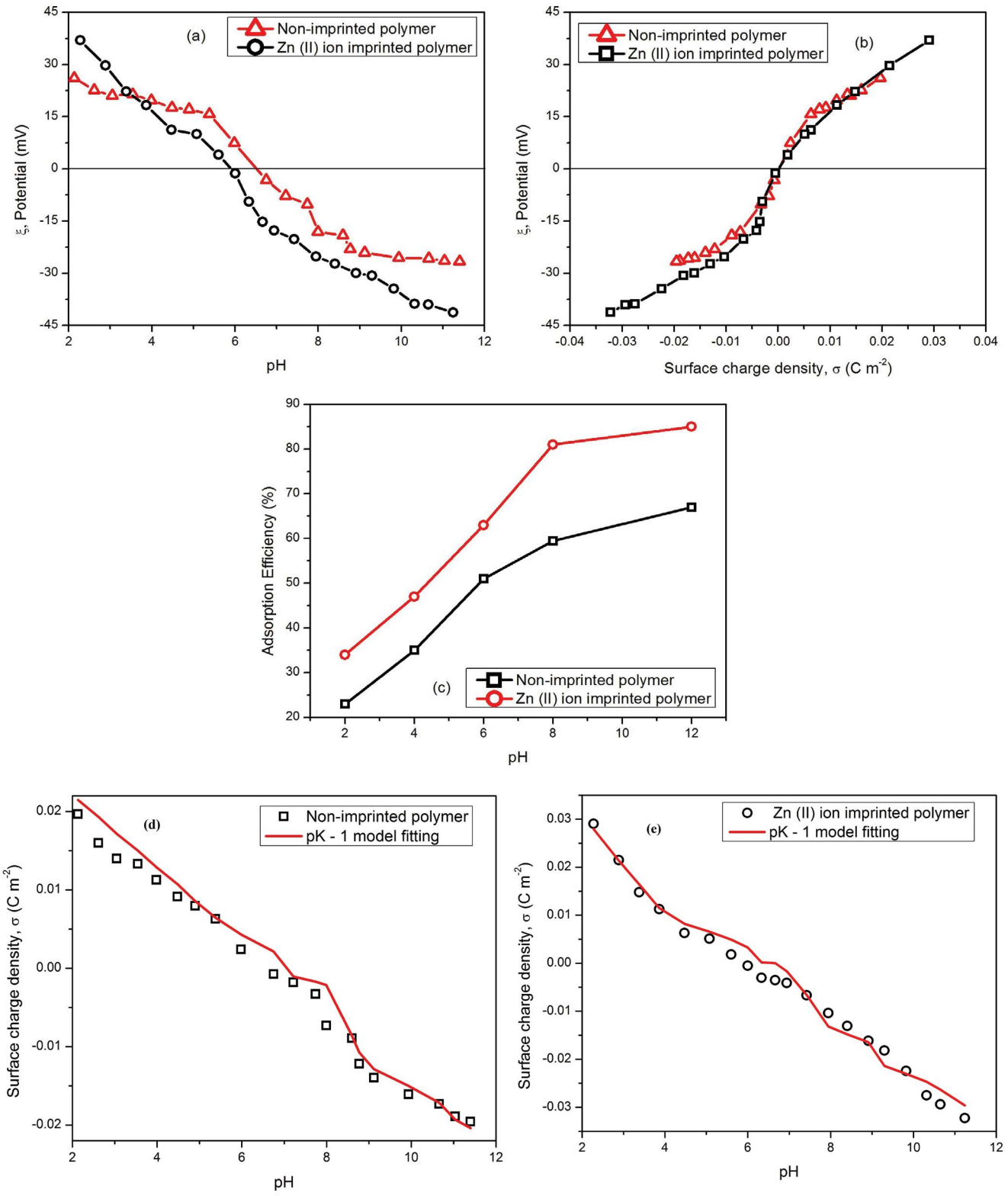

Fig. 6. (a) Point of zero charge pH_{pzc} measurement, (b) surface potential vs. surface charge, (c) depicts the influence of pH on the adsorption of Zn(II) ion on adsorbents; (d, e) pK-1 model fitting on NIP & Zn(II) IIP.

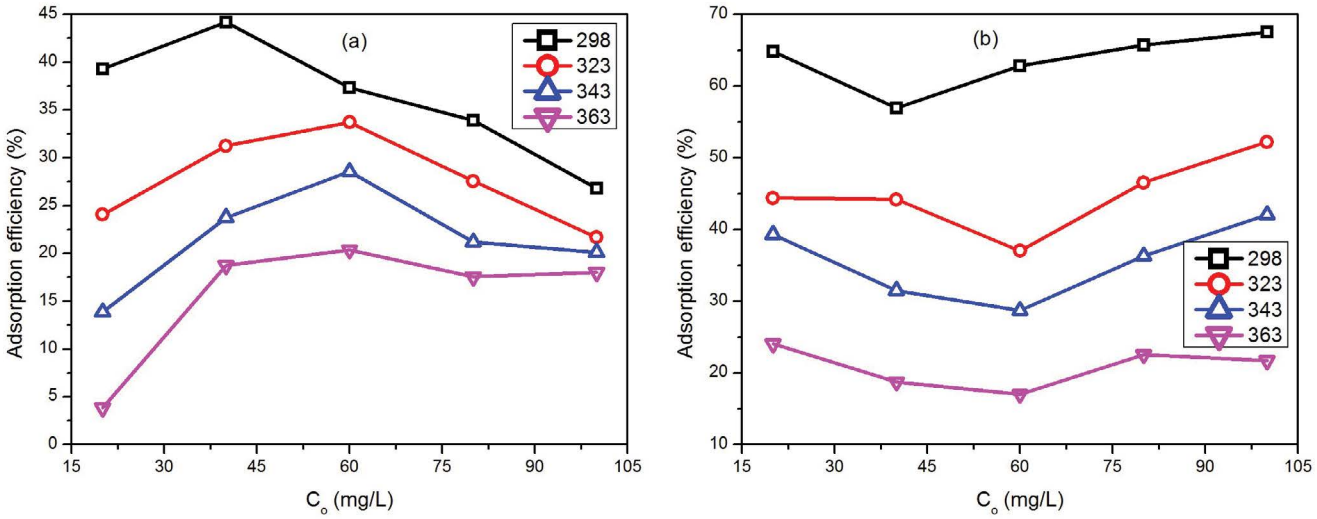

Fig. 7. Percent adsorption efficiency of adsorption of Zn(II) ions on (a) non-imprinted (NIP) and (b) Zn(II) ion-imprinted (IIP) polymer adsorbent at pH = 7.

efficiency showed decrease pointing to an inverse relation between temperature and adsorption efficiency for both Zn(II) IIP as well as NIP adsorbent. The adsorption efficiency showed decrease with the increase in temperature pointing to the exothermic nature of the adsorption of Zn(II) ions on both Zn(II) IIP and NIP adsorbent [46]. The imprinting phenomenon also results an increase in surface area due to mesoporosity which can be attributed to increase in the adsorption efficiency of Zn(II) IIP [47].

3.6. Equilibrium studies

For understanding the mechanism of adsorption of Zn(II) ions as adsorbate on NIP as well as Zn(II) IIP adsorbent, the plots of the adsorption capacity q_e against the equilibrium concentration C_e as shown in Fig. 8a and b, for equilibrium adsorption data were attained elaborating the adsorption isotherm models at four different temperatures. For calculating the adsorption capacity of the adsorbents, following equation was applied as

$$q_e = \frac{(C_o - C_e)V}{m} \tag{21}$$

where q_e is the adsorption capacity of Zn(II) ions on adsorbent (mg g^{-1}), V is the volume of Zn(II) ion solution (L) and m is the mass of adsorbent used (g). From the figure, it can be inferred that the adsorption capacity increases sharply with the increase in initial concentration until it reaches the point of saturation and also show decrease with the increase in the temperature pointing to exothermic nature of adsorption process. As compared to the NIP adsorbent, the maximum adsorption capacity was higher for Zn(II) IIP adsorbent depicting the mesoporous nature of the adsorbent as elaborated previously. The exothermic nature of the adsorption suggests that low temperature favours the adsorption of Zn(II) ions on the NIP as well as Zn(II) IIP which can be attributed to Zn(II) ions escaping from solid to liquid phase with temperature elevation resulting in adsorptive forces weakening. This corresponds directly to the phenomenon of chemical adsorption occurring simultaneously with physisorption having low heat of adsorption as signature [48]. In addition, the Zn(II) ions chelate with the electron donating group of 8-hydroxyquinoline which result in complementary cavities for the Zn(II) ions on the IIP adsorbent whereas incase of the NIP adsorbent, there are groups such as –NH and –C=O available for chelation.

Furthermore, the equilibrium adsorption data was fitted linearly with different isotherm models such as Langmuir, Freundlich and Dubinin–Radushkevich which revealed important parameters that elaborated the mechanism of the adsorption process.

For the adsorption occurring at the homogeneous active sites at the surface of the adsorbent leading to the monolayer adsorption, Langmuir isotherm model is applied which evaluate the adsorbate monolayer formation on identical sites and its linear empirical form is given as follows

$$\frac{C_e}{q_e} = \frac{1}{q_o K} + \frac{C_e}{q_o} \tag{22}$$

where C_e represents the equilibrium concentration of solute (mg L^{-1}), q_e represents the equilibrium solid-phase adsorption capacity (mg g^{-1}), K is the equilibrium adsorption constant (L mg^{-1}) and q_o illustrates the adsorbent maximum monolayer adsorption capacity (mg g^{-1}) [49]. The straight line plot of C_e/q_e vs. C_e gives the value of the maximum monolayer adsorption capacity from the slope $1/q_o$ whereas the equilibrium adsorption constant from the intercept $1/q_oK$ as represented in Fig. 9a and b. At 303 K, the adsorbent maximum monolayer adsorption capacity q_o for the NIP was 9.62 mg g^{-1} whereas its value was 23.29 mg g^{-1} for Zn(II) IIP. This means that the Zn(II) IIP adsorbent is more efficient in adsorption for Zn(II) adsorption as compared

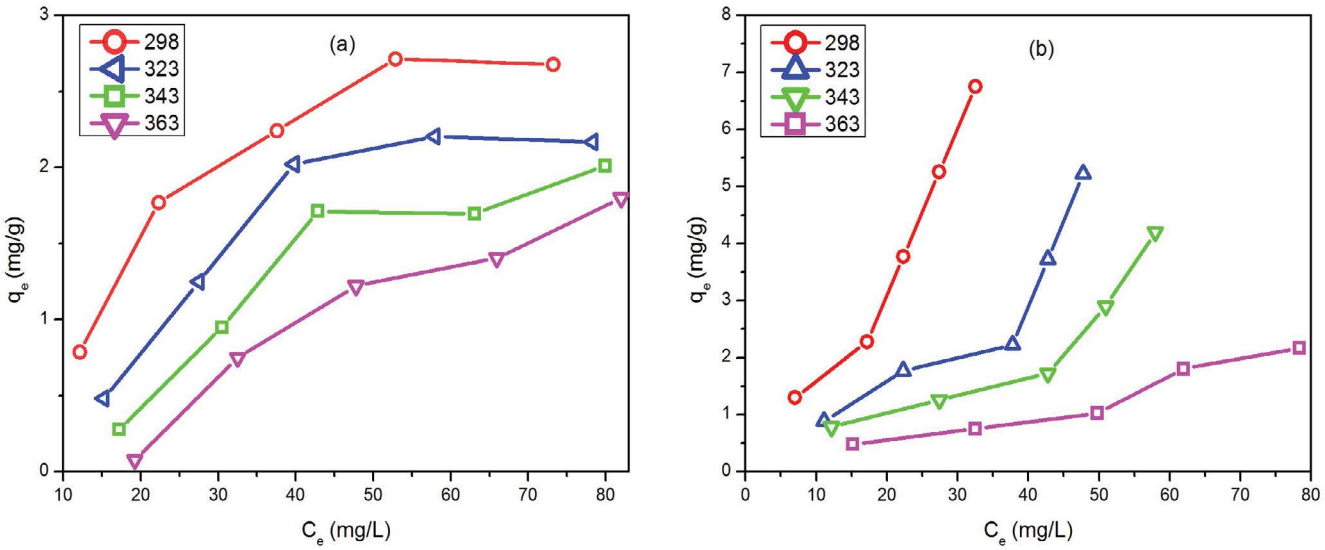

Fig. 8. Adsorption isotherm plot of q_e vs. C_e for the equilibrium adsorption data of adsorption of Zn(II) ions on (a) non-imprinted (NIP) and (b) Zn(II) ion-imprinted (IIP) polymer adsorbent at pH = 7.

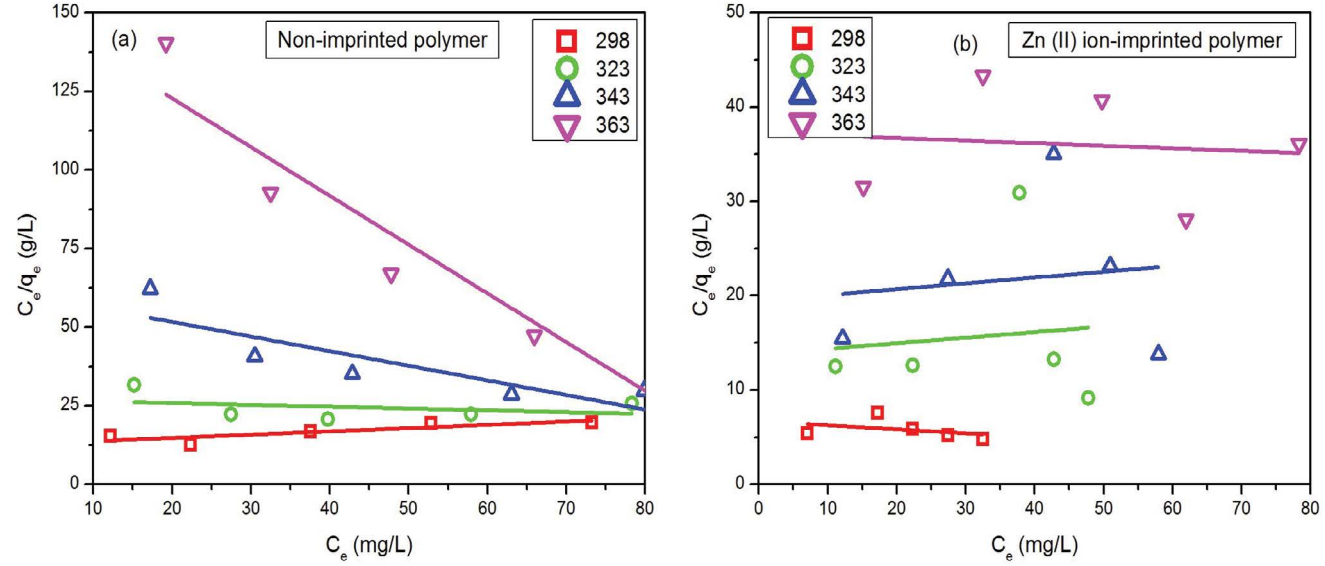

Fig. 9. Equilibrium adsorption data fitted with Langmuir adsorption isotherm model for adsorption of Zn(II) ions on (a) non-imprinted (NIP) and (b) Zn(II) ion-imprinted (IIP) polymer adsorbent.

to the NIP. In addition, the adsorbent maximum monolayer adsorption capacity q_o for the Zn(II) IIP for Zn(II) ion adsorption is higher as compared to the previous work performed by Supriyanto et al. [50] who reported a value of 20.83 mg g^{-1}, respectively. It can be depicted from this increase that the method adopted for imprinting was successful in creating cavities on the surface due to better interaction of the 8-hydroxyquinolinato-chelate complexes with the polymer matrix which resulted in leaving behind active sites after leaching resulting an efficient supported matrix that has potential to be applied in the separation process for the metal ions [46].

A dimensionless constant R_L is the separation factor derived from the Langmuir isotherm model equilibrium constant K. The value of R_L greater than 1 is indicative of the unfavourable adsorption mechanism whereas for $0 < R_L < 1$ depicts the favourable process of the physical adsorption. In addition, irreversible process of chemical adsorption occurs when $R_L = 0$ [51]. The equation for R_L factor is given as;

$$R_L = \frac{1}{1 + KC_0} \tag{23}$$

The R_L factor values were found within the favourable range of $0 < R_L < 1$ for four different temperatures as given in Table 2 depicting the favourability of occurrence of the physical adsorption at low temperature [52]. It is also worth noting to report here that the adsorbent maximum monolayer adsorption capacity q_o (mg g^{-1}) show increase with decrease in temperature which can be attributed to values of the R_L factor corresponding to the favourable nature of adsorption.

For the adsorbent surface possessing heterogeneous sites with different affinities for adsorption of adsorbate, the Freundlich adsorption isotherm is applied which suggests that sites with higher affinity are occupied primarily followed by adsorption at surface sites having less affinity [53]. Accordingly, this explains the gradual decrease in the adsorption capacity as the adsorbate concentrate at the active sites [54]. The empirical equation of the Freundlich isotherm is given in its linear logarithmic form as:

$$\ln q_e = \ln K_f + \left(\frac{1}{n}\right)\ln C_e \tag{24}$$

where K_f is the Freundlich adsorption constant indicating the adsorption capacity (mg g^{-1})/(L mg^{-1}) attained from the intercept of the straight line graph of $\ln q_e$ vs. $\ln C_e$ whereas the slope provides the value of $1/n$ depicting the adsorption intensity, referred to as the exponent of non-linearity, respectively as shown in Fig. 10a and b. For higher values of K_f corresponds to significant occurrence of the adsorption and its decrease with increase in temperature points to decrease in adsorption due to exothermic nature [55,56]. If the value of $1/n < 1$, then there is a strong interaction between adsorbate and adsorbent as the adsorption process becomes less desirable with the rise in $1/n$ value. The higher adsorption for the lower values of $1/n$ points to the fact that adsorption process is significant due to strong interaction between adsorbate and adsorbent which results in q_e less dependent on the C_e leading to adsorption process enhancement [57]. The lower values of $1/n$ at lower temperature elaborate the enhanced adsorption due to exothermic nature of the adsorption process for Zn(II) ions on NIP whereas for Zn(II) IIP adsorbent, the $1/n$ values first show decrease followed by increase suggesting an irregular behavior as function of temperature.

Table 2 evaluates the parameters of Langmuir and Freundlich adsorption isotherm models showing the correlation factor R^2 of Freundlich isotherm model for both Zn(II) IIP and NIP in the range of 0.843–0.989 and 0.468–0.913 respectively which are higher as compared to the R^2 values of Langmuir isotherm model suggesting that the Freundlich adsorption isotherm for of Zn(II) ions adsorption is followed more closely depicting the heterogeneity of the adsorbent surface [58].

Dubinin–Radushkevich isotherm in its linear logarithmic form is given as;

$$\ln q_e = \ln q_m + K'\varepsilon^2 \tag{25}$$

where q_e denotes the equilibrium adsorption capacity (mg g^{-1}), q_m represents the maximum monolayer adsorption capacity of adsorbent (mg g^{-1}) assuming the surface to be microporous in nature [59], ε is the Polanyi potential and K' is the adsorption energy constant ($mol^2\ kJ^{-2}$) [60]. The slope of the plot of $\ln q_e$ vs. ε^2 gives the value of K' whereas the intercept provides the value of q_m as shown in Fig. 11a and b. Polanyi potential ε explains the adsorption dependence on temperature by using the adsorbate equilibrium concentration C_e (mg L^{-1}) in the following form given as:

$$\varepsilon = RT\ln\left(1+\frac{1}{C_e}\right) \tag{26}$$

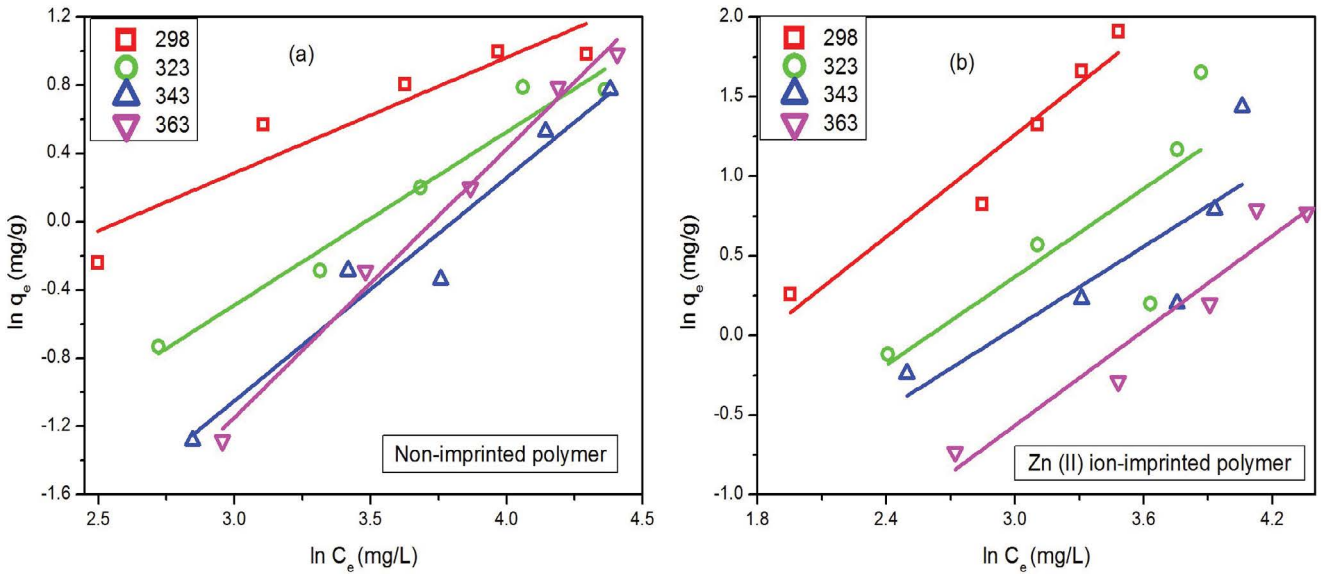

Fig. 10. Equilibrium adsorption data fitted with Freundlich adsorption isotherm model for adsorption of Zn(II) ions on (a) non-imprinted (NIP) and (b) Zn(II) ion-imprinted (IIP) polymer adsorbent.

Table 2
Values of various applied adsorption isotherm model parameters for adsorption of Zn(II) ions (a) non-imprinted (NIP) and (b) Zn(II) ion-imprinted (IIP) polymer adsorbent at different temperatures

Adsorption isotherm equation		Langmuir			
Adsorbent	T (K)	q_o (mg g^{-1})	K (L mg^{-1})	R_L	R^2
NIP	298	9.620	0.0082	0.924	0.6271
	323	–17.372	–0.002	1.022	–0.187
	343	–2.150	–0.008	1.083	0.6361
	363	–0.646	–0.010	1.112	0.8652
IIP	298	–23.283	–0.006	1.068	–0.127
	323	16.992	0.004	0.959	–0.319
	343	16.129	0.003	0.969	–0.308
	363	–36.549	–0.001	1.008	–0.317

Adsorption isotherm equation		Freundlich		
Adsorbent	T (K)	K_f ((mg g^{-1})/(L mg^{-1}))	$1/n$	R^2
NIP	298	0.174	0.677	0.843
	323	0.029	1.016	0.946
	343	0.007	1.307	0.933
	363	0.003	1.574	0.989
IIP	298	0.143	1.067	0.913
	323	0.091	0.923	0.468
	343	0.082	0.851	0.595
	363	0.029	0.993	0.904

Adsorption isotherm equation		Dubinin–Radushkevich			
Adsorbent	T (K)	K' (mol^2 kJ^{-2})	E (kJ mol^{-1})	q_m (mg g^{-1})	R^2
NIP	298	–31.66	0.126	2.723	0.986
	323	–50.79	0.099	1.856	0.719
	343	–72.42	0.083	1.625	0.759
	363	–95.53	0.073	2.287	0.885
IIP	298	–12.58	0.199	4.923	0.647
	323	–23.23	0.147	2.894	0.309
	343	–21.76	0.152	2.210	0.319
	363	–37.25	0.116	1.719	0.611

where R is the universal gas constant. The increase in the values of the ε depicts the increase in adsorption efficiency due to decrement in the C_e value. The mean adsorption energy E (kJ mol^{-1}) value points to the adsorption nature being physical or chemical and is correlated to adsorption energy constant K' as;

$$E = \frac{1}{\left(2K'\right)^{\frac{1}{2}}} \tag{27}$$

When physical adsorption occurs, E < 8 kJ mol^{-1}, whereas E = 8–16 kJ mol^{-1} corresponds to chemical adsorption respectively [61]. For the adsorption of the Zn(II) ions on both the NIP as well as Zn(II) IIP adsorbents, the E values suggests the occurrence of the chemisorption corresponding to monolayer formation as the adsorbate chelate with the surface actives sites of adsorbent. The decrease in the E values with the increase in the temperature also confirms the hypothesis of exothermic chemisorption occurrence.

3.6. Adsorption thermodynamics

The change in the Gibbs free energy (ΔG), entropy (ΔS), and enthalpy (ΔH) are the parameters of thermodynamics used in order to study the equilibrium adsorption process of Zn(II) ions on both NIP as well as Zn(II) IIP with respect to temperature. For evaluating the thermodynamic parameters, Van't Hoff equation is applied which integrates the absolute temperature (T) to the adsorption equilibrium constant (K) that is attained from the Langmuir adsorption isotherm model respectively. The logarithmic linear Van't Hoff expression is given as [62];

$$\ln K = \left(\frac{\Delta S}{R}\right) - \left(\frac{\Delta H}{RT}\right) \tag{28}$$

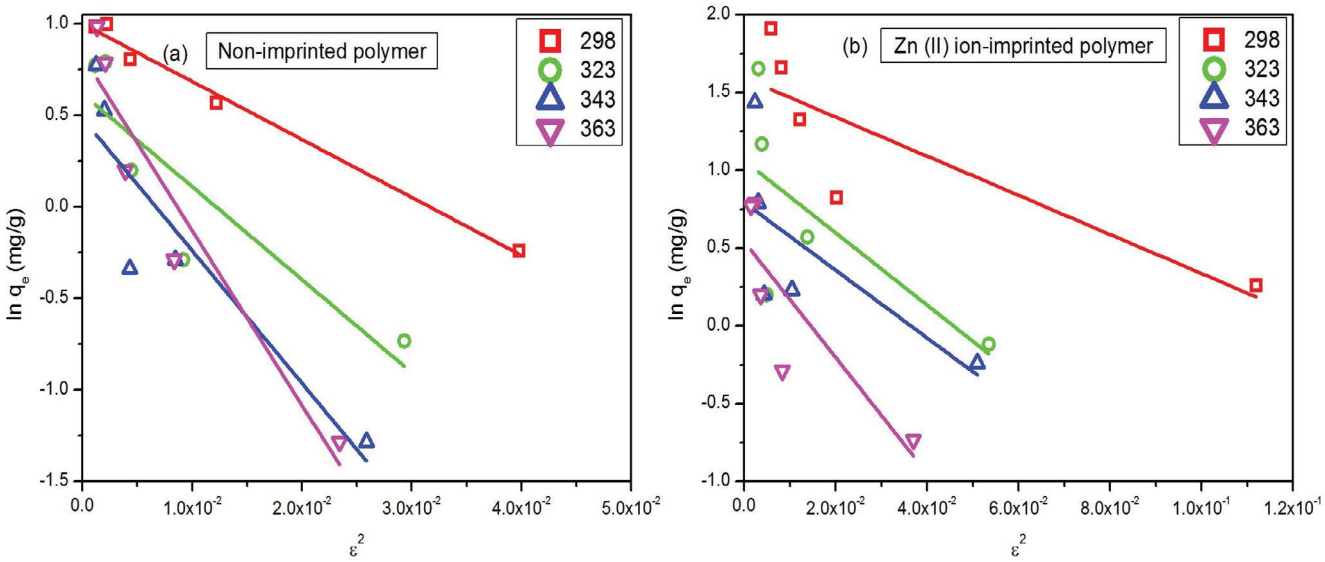

Fig. 11. Equilibrium adsorption data fitted with Dubinin–Radushkevich adsorption isotherm model for adsorption of Zn(II) ions on (a) non-imprinted (NIP) and (b) Zn(II) ion-imprinted (IIP) polymer adsorbent.

The slope and intercept of the linear plot of ln$K$ vs. 1/T as shown in Fig. 12, is used to find the change in enthalpy (ΔH) and entropy (ΔS), respectively, whereas Gibbs free energy change (ΔG) is determined by the equation given below as [63];

$$\Delta G = \Delta H - T\Delta S \tag{29}$$

At equilibrium, ΔG as the driving force is related to the adsorption equilibrium constant K as the standard Gibbs free energy change $\Delta G°$ is inherently equal to zero and ΔG is given at equilibrium by the following equation as;

$$\Delta G = -RT\ln K \tag{30}$$

So according to the calculated values of the thermodynamic parameters as shown in Table 3 for both NIP as well as Zn(II) IIP, ΔH values are negative indicating the exothermic nature of adsorption for the adsorption of Zn(II) ions [64]. The positive value for entropy change (ΔS) suggests that there is no thermodynamic barriers for the Zn(II) ions adsorption on adsorbent indicating the spontaneous nature of adsorption which cause an increase in the randomness of the adsorption process [65]. The negative value of ΔG suggests that the spontaneous adsorption process of Zn(II) ions on both NIP as well as Zn(II) IIP occurs which further increases with an increase in the temperature indicating the exothermic nature of adsorption of Zn(II) ions on NIP whereas for Zn(II) IIP adsorbent, a decrease is observed pointing to the endothermic nature of adsorption [26].

3.7. Adsorption kinetic studies

The kinetic models of pseudo-first-order, pseudo-second-order and intraparticle diffusion were applied to study the adsorption kinetics. The linear equations for these models are given as;

Pseudo-first-order kinetic model is [66];

$$\ln\left(q_e - q_t\right) = \ln q_e - k_1 t \tag{31}$$

Pseudo-second-order kinetic model is [67];

$$\frac{t}{q_t} = \frac{1}{k_2 q_e^2} + \frac{t}{q_e} \tag{32}$$

where q_e is the quantity of Zn(II) adsorbed at equilibrium, q_t is the binding capacity of Zn(II) ion at time t, k_1 and k_2 are representing the rate constant of the kinetics models respectively. The value of k_1 is determined from the slope of the plot of $\ln(q_e - q_t)$ vs t for pseudo-first-order kinetic model as shown in Fig. 13a and b whereas the k_2 value is determined from the intercept of the plot of t/q_t against t as given in Fig. 14a and b. The values for the various kinetic parameters determined after linear fitting of the pseudo-first-order and pseudo-second-order kinetics are given in Table 4. The value of the co-relation factor R^2 of pseudo-first-order kinetics for both on NIP as well as Zn(II) IIP are in the range 0.784–0.951 and 0.897–0.976 respectively, as compared to the R^2 values for pseudo-second-order kinetics which are in the range of –0.055–0.591 and 0.024–0.997 for both polymeric adsorbents. By the comparison of the R^2 values of both kinetic models, it is apparent that the adsorption of Zn(II) ions obeys the pseudo-first-order kinetic pointing to the fact that there is a physical interaction between the Zn(II) ions and adsorbent and hence only substrate dependent adsorption process occurs since this kinetic model does not take into consideration the diffusion that occur through the boundary as it suggests a one step process for the adsorption [68]. Similarly, the

theoretical value of $q_{e,cal}$ for pseudo-first-order kinetics for the adsorption of Zn(II) ions for both on NIP as well as Zn(II) IIP resembles the experimental q_e as it does consider the interaction between solvent and adsorbate. However, the theoretical value of $q_{e,cal}$ for pseudo-second-order kinetics is not quite close to the experimental q_e which suggests that the adsorption kinetics of Zn(II) ions does not follow the pseudo-second-order kinetic, which can be attributed to the less chemical interaction between the Zn(II) ions and adsorbent leaving the option of the chemisorption as rate limiting step [69]. Hence it is both substrate and adsorbate dependent adsorption process [70]. The initial concentration of adsorbate in addition to the adsorbent nature does influence the process of adsorption which can also be responsible for the adsorption capacity experimental and calculated values difference [71]. Furthermore, it can be stated that adsorption phenomenon in the liquid–solid phase occurs in multiple steps which depends upon either pore dimension, surface diffusion, film formation or heterogeneous sites of the pores

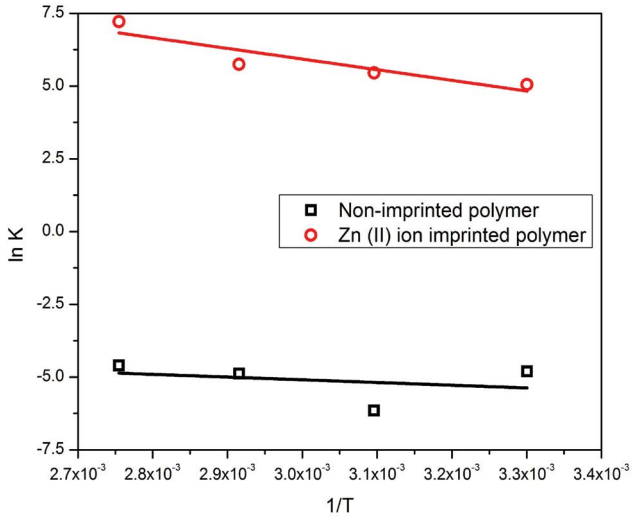

Fig. 12. Logarithmic linear plot of ln$K$ vs. 1/T for the thermodynamic parameters evaluation of adsorption of Zn(II) ions on non-imprinted (NIP) and Zn(II) ion-imprinted polymer (IIP) adsorbent.

where adsorption occurs as whichever may be the limiting step or the process may comprise multiple steps [72,73].

The intraparticle diffusion model elaborates the rate of adsorption which considers the diffusion of adsorbate towards surface of the adsorbent as rate limiting step for which the linear equation is given as [74];

$$q_t = k_i t^{\frac{1}{2}} + C \tag{33}$$

where q_t is the quantity of Zn(II) ions adsorbed at equilibrium and k_i is representing the rate constant of the intraparticle diffusion model of kinetics. This model is based on the hypothesis that the spreading of liquid film formed in the mobile phase has an affect only on the starting time period of the adsorption phenomenon and can be ignored. This model is basically applicable for those adsorbents which are porous in nature. Plot of $t^{1/2}$ and q_t as shown in Fig. 15a and b have three definite segments, that is, (i) the part at which the adsorption rate is very high known as bulk diffusion, points to the starting bend or sharp-sloped part, (ii) the intraparticle diffusion part is associated with the following linear part, and (iii) the last segment directing the equilibrium is known as plateau part. Plot of $t^{1/2}$ and q_t was used to determine the value of C from the intercept which indicates the boundary layer thickness, whereas the rate constant k_i is attained from the slope [75]. The assumption of this model is that if $t^{1/2}$ vs. q_t gave a straight line plot along with passing through the origin, then it would also be an indication that this model depicts the rate determining step too. The evaluated parameters of the intraparticle diffusion model as given in Table 4, concludes the fact that the adsorption kinetic data was well fitted linearly with this model, hence this model is followed in the adsorption process. Since the graph didn't pass through the origin so, it is suggested that it was not a slow step known as rate determining step [76].

3.8. Adsorption activation energy

Arrhenius equation was used to evaluate the activation energy for the Zn(II) ions adsorption on both NIP and Zn(II) IIP. Since the adsorption kinetics followed the pseudo-first-order kinetics, hence the rate constant k_1 was used to calculate the activation energy E_a parameter which

Table 3
Thermodynamic parameters of ΔG, ΔS, and ΔH

Adsorbent	ΔH (kJ mol^{-1})	ΔS (kJ mol^{-1})	T (K)	ΔG (kJ mol^{-1})
	–0.11	–0.0003	298	–0.021
			323	–0.015
NIP			343	–0.009
			363	–0.003
IIP	–0.44	0.002	298	–1.046
			323	–1.086
			343	–1.126
			363	–1.166

Table 4
Comparison of kinetic models pseudo-first-order, pseudo-second-order and intraparticle diffusion model for adsorption of Zn(II) ions on (a) non-imprinted (NIP) and (b) Zn(II) ion-imprinted polymer (IIP) adsorbent at different temperatures

Adsorption kinetic model for adsorption of							
		T (K)	$q_{e,exp}$ (mg g^{-1})	$q_{e,cal}$ (mg g^{-1})	k_1 (1 min^{-1})	R^2	
Pseudo-first-order kinetic model	NIP	298	3.695	3.972	0.022	0.869	
		323	3.012	2.767	0.006	0.784	
		343	2.241	2.392	0.015	0.952	
		363	2.037	2.029	0.015	0.942	
	IIP	298	7.401	10.047	0.022	0.913	
		323	5.168	3.843	0.014	0.976	
		343	4.203	2.528	0.012	0.905	
		363	3.749	5.054	0.019	0.897	
		T (K)	$q_{e,exp}$ (mg g^{-1})	$q_{e,cal}$ (mg g^{-1})	k_2 (g gm^{-1} min^{-1})	R^2	
Pseudo-second-order kinetic model	NIP	298	3.695	–1.776	0.0024	–0.054	
		323	3.012	2.457	0.0057	0.590	
		343	2.241	5.487	0.0006	0.123	
		363	2.037	5.119	0.0007	0.246	
	IIP	298	7.401	10.82	0.0009	0.814	
		323	5.168	5.518	0.0054	0.958	
		343	4.203	4.247	0.0091	0.996	
		363	3.749	7.522	0.0006	0.024	
		T (K)	$q_{e,exp}$ (mg g^{-1})	$q_{e,cal}$ (mg g^{-1})	k_i (mg g^{-1} min^{-1})	C (mg g^{-1})	R^2
Intraparticle diffusion model	NIP	298	3.695	7.845	0.043	0.375	0.590
		323	3.012	6.382	0.017	0.449	0.862
		343	2.241	8.341	0.020	0.368	0.862
		363	2.037	4.679	0.020	0.322	0.823
	IIP	298	7.401	9.341	0.069	1.433	0.914
		323	5.168	6.347	0.033	1.993	0.908
		343	4.203	2.879	0.026	1.680	0.664
		363	3.749	4.786	0.035	0.493	0.852

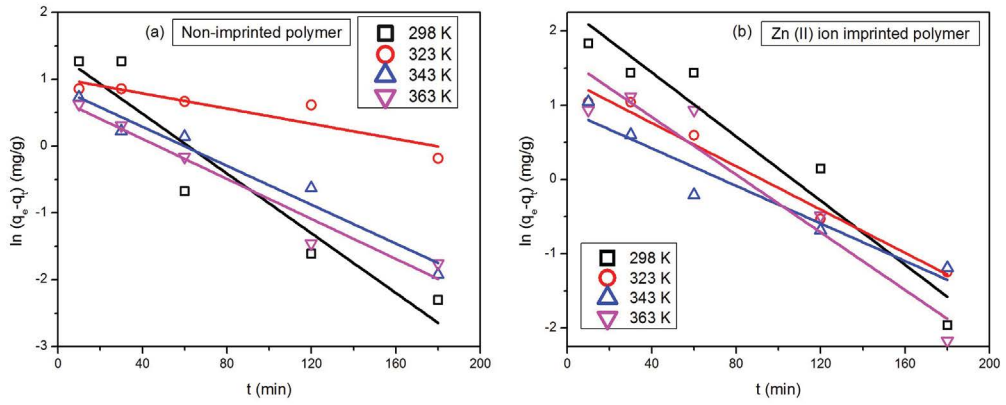

Fig. 13. Pseudo-first-order model applied on kinetic data of adsorption of Zn(II) ions on (a) non-imprinted (NIP) and (b) Zn(II) ion-imprinted polymer (IIP) adsorbent at different temperatures.

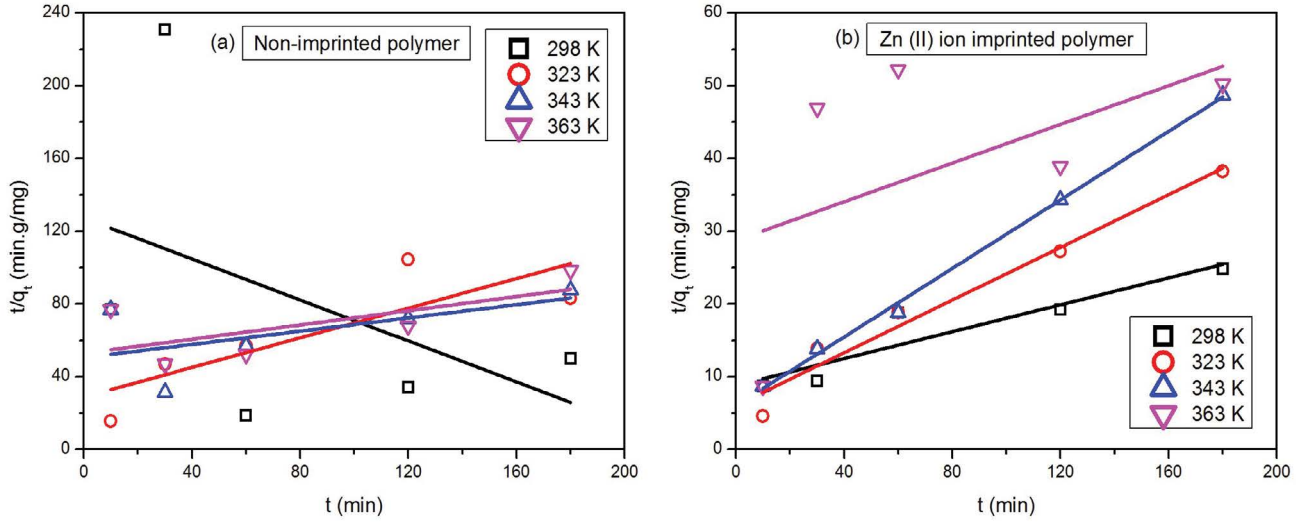

Fig. 14. Pseudo-second-order model applied on kinetic data of adsorption of Zn(II) ions on (a) non-imprinted (NIP) and (b) Zn(II) ion-imprinted polymer (IIP) adsorbent at different temperatures.

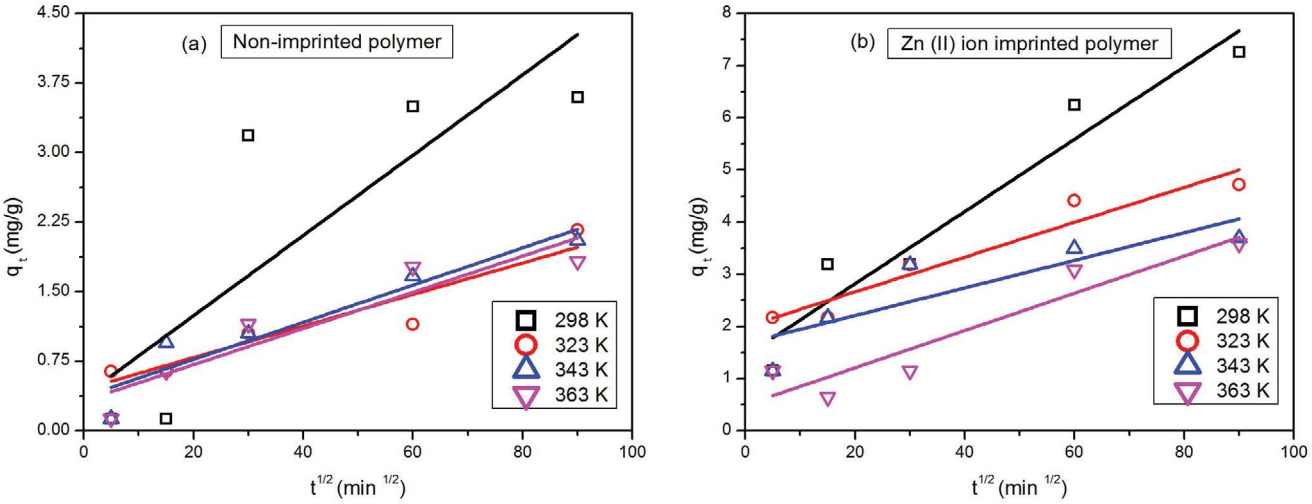

Fig. 15. Intraparticle diffusion model applied on kinetic data of adsorption of Zn(II) ions on (a) non-imprinted (NIP) and (b) Zn(II) ion-imprinted polymer (IIP) adsorbent at different temperatures.

was attained from the slope of the plot of ln$K$ vs. $1/T$ as shown in Fig. 16 using the equation given below:

$$\ln k = \ln A - \frac{E_a}{RT} \tag{34}$$

where A is Arrhenius constant (g mg^{-1} min^{-1}), E_a is activation energy (kJ mol^{-1}), R is real gas constant (8.314 J mol^{-1}) and T is absolute temperature (K). In order to differentiate between the physisorption and chemisorption phenomenon, the value of activation energy has been commonly used, since easily reversible phenomenon is physisorption which must have small activation energy value. In contrast, chemisorption is due to strong force of attraction specifically when it is the involvement of chemical bonds which can't be reversed easily, hence must have large activation energy values. The standard values of activation energy E_a set for physisorption and chemisorption phenomenon are in the range of 5–40 kJ mol^{-1} and 40–800 kJ mol^{-1}, respectively. As shown in Table 5, the activation energy (E_a) value for both NIP and Zn(II) IIP lies below 40 kJ mol^{-1}, that is 0.026 and 0.046 kJ mol^{-1} respectively, pointing to the fact that there are weak Van der Waals force of attraction between the Zn(II) ions and adsorbent, hence suggesting the occurrence of the physisorption phenomenon [77].

3.9. Selectivity study

For carrying out the competitive adsorption, the mixture of each metal ion with Zn(II) ion such as Zn(II)/Cu(II),

Zn(II)/Co(II), Zn(II)/Ni(II) and Zn(II)/Pb(II) is employed using NIP and Zn(II) IIP as adsorbents. The interfering metal ions have similarity with respect to charge and ionic radii to the Zn(II) ions, respectively. The $K_{d\ (IIP)}$ values of Zn(II) IIP for Zn(II) are higher in comparison with the interfering metals of Pb(II), Co(II), Cu(II), and Ni(II) as listed in Table 6. Since, the actives sites created on Zn(II) IIP after the template removal were complementing in shape, size, charge and coordination symmetry to the imprinted ion only due to which it has high k values as compared to NIP which has low k value that can be attributed to the random arrangement of functional groups of ligand in the cross-linked polymeric network. It is apparent that Zn(II) ions are adsorbed to greater extent on the Zn(II) IIP due to higher selectivity especially for Zn(II) ion.

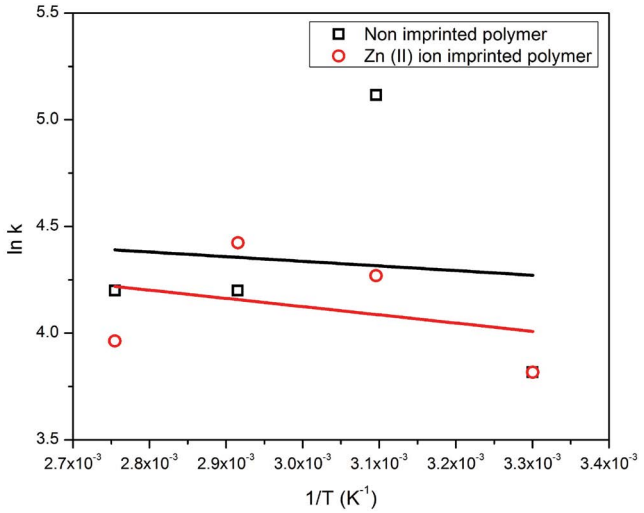

Fig. 16. Activation energy plot for adsorption of Zn(II) ions on non-imprinted (NIP) and Zn(II) ion-imprinted polymer (IIP) adsorbent.

Table 5
Comparison of activation energy E_a and Arrhenius constant A of Arrhenius equation applied to kinetic data of adsorption of Zn(II) ions on non-imprinted (NIP) and Zn(II) ion-imprinted polymer (IIP) adsorbent

Adsorbents	A (g mg^{-1} min^{-1})	E_a (kJ mol^{-1})	R^2
NIP	146.6	0.026	0.008
IIP	195.6	0.046	0.106

3.7. Desorption

It is apparent from Fig. 6, that with the decrease in pH value, the positively charged sites will appear predominantly on the adsorbent surface which will attribute to the decrease in the Zn(II) ions interaction with the active sites. Therefore, in order to perform elution so that the adsorbent is regenerated, 0.1 N solution of HCl was applied as eluting agent which will result in metal ion leaching from both the adsorbents. The data for the Zn(II) ion desorption is listed in Table 7.

4. Conclusion

The adsorption equilibrium data shows that there is a noticeable increase in the adsorption capacity of the Zn(II) IIP as compared to NIP which can be attributed to the increase in the occurrence of active sites at the surface leading to the surface area increase which enhances the adsorption phenomenon. The determination of the pH_{pzc} elaborates the pH effect on the adsorption efficiency since at higher pH the adsorbent efficiency is high which is due to anionic nature of surface of adsorbent. The pH value increase results an increase in the negative charge on the adsorbent surface due to which the positively charged Zn(II) ion forms complex with active sites on the surface of adsorbent leading to an increase in the adsorption efficiency. The adsorption equilibrium data was best fit with Freundlich adsorption model suggesting the homogeneous nature of adsorbent surface. The surface area analysis by BET show an increase from 337.30 m^2 g^{-1} for NIP to 439.54 m^2 g^{-1} for Zn(II) IIP which is due to formation of active sites at the surface due to imprinting whereas an increase in the mesoporosity is observed by t-plot and BJH model as apparent due to increase in the mesopore volume from 32.56 m^2 g^{-1} for NIP to 43.95 m^2 g^{-1} for Zn(II) IIP which is responsible for increase in adsorption efficiency as well. The spontaneity of the process as indicated by Gibbs free energy negative value reduces at elevated temperature while following the thermodynamic study at the different temperature makes it clear that the adsorption process is an exothermic process. Similarly, the kinetic study does indicate that the rate of adsorption is controlled by the rate limiting step of diffusion confirming the occurrence of adsorption in more

Table 6
Comparison of selectivity of non-imprinted (NIP) and Zn(II) ion-imprinted polymer (IIP) adsorbent for adsorption of Zn(II) ions

Metal type	Zn(II) IIP		NIP		
	K_d (mL g^{-1})	k	K_d (mL g^{-1})	k	k'
Zn(II)	32.822		17.532		
Co(II)	0.892	36.795	11.821	1.482	24.827
Cu(II)	21.749	1.509	14.798	1.185	1.273
Ni(II)	12.684	2.587	26.617	0.658	3.931
Pb(II)	17.463	1.879	22.754	0.771	2.437

Table 7
Comparison of desorption of Zn(II) ions from loaded non-imprinted (NIP) and Zn(II) ion-imprinted polymer (IIP) adsorbent using 0.1 mol L^{-1} HCl aqueous solution as eluent

Zn(II) ions added (μg)	Zn(II) ions eluted (μg) (NIP)	Desorption %	Zn(II) ions eluted (μg) (IIP)	Desorption %
200	149.623	74.854	164.937	82.567
400	329.851	82.576	342.865	85.774
600	515.727	85.992	531.843	88.667

than one step. The low value of the adsorption activation energy points to the physical nature of the adsorption.

Acknowledgement

This research did not receive any specific funding. The authors declare no conflicts of interest

References

[1] R. Henkel, J. Bittner, R. Weber, F. Hüther, W. Miska, Relevance of zinc in human sperm flagella and its relation to motility, Fertil. Steril., 71 (1999) 1138–1143.
[2] R.J. Cousins, A role of zinc in the regulation of gene expression, Proc. Nutr. Soc., 57 (1998) 307–311.
[3] M.J. Kuras, K. Perz, W.L. Kołodziejski, Synthesis, characterization and application of a novel zinc(II) ion-imprinted polymer, Polym. Bull., 74 (2017) 5029–5048.
[4] L.M. Plum, L. Rink, H. Haase, The essential toxin: impact of zinc on human health, Int. J. Environ. Res. Public Health, 7 (2010) 1342–1365.
[5] S.D. Kolev, Y. Baba, R.W. Cattrall, T. Tasaki, N. Pereira, J.M. Perera, G.W. Stevens, Solid phase extraction of zinc(II) using a PVC-based polymer inclusion membrane with di(2-ethylhexyl)phosphoric acid (D2EHPA) as the carrier, Talanta, 78 (2009) 795–799.
[6] S. Vellaichamy, K. Palanivelu, Preconcentration and separation of copper, nickel and zinc in aqueous samples by flame atomic absorption spectrometry after column solid-phase extraction onto MWCNTs impregnated with D2EHPA-TOPO mixture, J. Hazard. Mater., 185 (2011) 1131–1139.
[7] Y. Cui, X. Chang, X. Zhu, H. Luo, Z. Hu, X. Zou, Q. He, Chemically modified silica gel with *p*-dimethylaminobenzaldehyde for selective solid-phase extraction and preconcentration of Cr(III), Cu(II), Ni(II), Pb(II) and Zn(II) by ICP-OES, Microchem. J., 87 (2007) 20–26.
[8] J. Zhao, B. Han, Y. Zhang, D. Wang, Synthesis of Zn(II) ion-imprinted solid-phase extraction material and its analytical application, Anal. Chim. Acta, 603 (2007) 87–92.
[9] S.M. El-Bahy, Z.M. El-Bahy, Immobilization of 2-amino pyridine onto poly(acrylonitrile-co-N,N′-methylenebisacrylamide) nanoparticles for the removal of Hg(II), Cd(II) and Cr(III): batch and column techniques, J. Environ. Chem. Eng., 5 (2017) 3560–3571.
[10] H. Yu, P. Shao, L. Fang, J. Pei, L. Ding, S.G. Pavlostathis, X. Luo, Palladium ion-imprinted polymers with PHEMA polymer brushes: role of grafting polymerization degree in anti-interference, Chem. Eng. J., 359 (2019) 176–185.
[11] P. Shao, D. Liang, L. Yang, H. Shi, Z. Xiong, L. Ding, X. Yin, K. Zhang, X. Luo, Evaluating the adsorptivity of organo-functionalized silica nanoparticles towards heavy metals: quantitative comparison and mechanistic insight, J. Hazard. Mater., 387 (2020) 121676, doi: 10.1016/j.jhazmat.2019.121676.
[12] Q.T. Yang, Q.L. Xie, N.C. Chen, Y.J. Zhong, Research progress on wastewater treatment by heavy metal ion-imprinted polymer, Mater. Sci. Forum, 921 (2018) 35–39.
[13] S. Jakavula, N. Raphael Biata, K. Mogolodi Dimpe, V.E. Pakade, P.N. Nomngongo, A critical review on the synthesis and application of ion-imprinted polymers for selective preconcentration, speciation, removal and determination of trace and essential metals from different matrices, Crit. Rev. Anal. Chem., 52 (2022) 314–326.
[14] Y. Wen, L. Chen, J. Li, D. Liu, L. Chen, Recent advances in solid-phase sorbents for sample preparation prior to chromatographic analysis, TrAC, Trends Anal. Chem., 59 (2014) 26–41.
[15] K.K. Jinadasa, E. Peña-Vázquez, P. Bermejo-Barrera, A. Moreda-Piñeiro, New adsorbents based on imprinted polymers and composite nanomaterials for arsenic and mercury screening/speciation: a review, Microchem. J., 156 (2020) 104886, doi: 10.1016/j.microc.2020.104886.
[16] L. Chen, J. Dai, B. Hu, J. Wang, Y. Wu, J. Dai, M. Meng, C. Li, Y. Yan, Recent progresses on the adsorption and separation of ions by imprinting routes, Sep. Purif. Rev., 49 (2020) 265–293.
[17] M. Li, X. Meng, X. Liang, J. Yuan, X. Hu, Z. Wu, X. Yuan, A novel In(III) ion-imprinted polymer (IIP) for selective extraction of In(III) ions from aqueous solutions, Hydrometallurgy, 176 (2018) 243–252.
[18] J. Kelson, R. Shamberger, Methods compared for determining zinc in serum by flame atomic absorption spectroscopy, Clin. Chem., 24 (1978) 240–244.
[19] J. Smith Jr., G. Butrimovitz, W. Purdy, Direct measurement of zinc in plasma by atomic absorption spectroscopy, Clin. Chem., 25 (1979) 1487–1491.
[20] J. Fu, L. Chen, J. Li, Z. Zhang, Current status and challenges of ion imprinting, J. Mater. Chem. A, 3 (2015) 13598–13627.
[21] W.J. Cheong, S.H. Yang, F. Ali, Molecular imprinted polymers for separation science: a review of reviews, J. Sep. Sci., 36 (2013) 609–628.
[22] H.M. Kwaambwa, A.R. Rennie, Interactions of surfactants with a water treatment protein from *Moringa oleifera* seeds in solution studied by zeta-potential and light scattering measurements, Biopolymers, 97 (2012) 209–218.
[23] A. Elaissari, Colloidal Polymers: Synthesis and Characterization, CRC press, Florida, 2003.
[24] G. Bolt, Determination of the charge density of silica sols, J. Phys. Chem., 61 (1957) 1166–1169.
[25] G.A. Parks, P.D. Bruyn, The zero point of charge of oxides1, J. Phys. Chem., 66 (1962) 967–973.
[26] T. ul Haq Zia, A.H. Mehmood, B. Ara, K. Gul, Investigation of the equilibrium, thermodynamic and kinetic parameters of study of the Allura red dye efficient removal from aqueous solution by magnetic α-Fe_2O_3 nanoparticles and its nanocomposite with graphite powder (α-Fe_2O_3/G-p), Desal. Water Treat., 139 (2019) 174–190.
[27] A.R. Kul, H. Koyuncu, Adsorption of Pb(II) ions from aqueous solution by native and activated bentonite: kinetic, equilibrium and thermodynamic study, J. Hazard. Mater., 179 (2010) 332–339.
[28] S.M. El-Bahy, Z.M. El-Bahy, Synthesis and characterization of polyamidoxime chelating resin for adsorption of Cu(II), Mn(II) and Ni(II) by batch and column study, J. Environ. Chem. Eng., 4 (2016) 276–286.
[29] G. Liu, X. Yang, Y. Wang, Silica/poly(N,N′-methylene-bisacrylamide) composite materials by encapsulation based on a hydrogen-bonding interaction, Polymer, 48 (2007) 4385–4392.
[30] F. Dellisanti, V. Minguzzi, G. Valdrè, Thermal and structural properties of Ca-rich montmorillonite mechanically deformed by compaction and shear, Appl. Clay Sci., 31 (2006) 282–289.

[31] N. Khaorapapong, M. Ogawa, *In-situ* formation of bis (8-hydroxyquinoline) zinc(II) complex in the interlayer spaces of smectites by solid–solid reactions, J. Phys. Chem. Solids, 69 (2008) 941–948.
[32] R.G. Charles, H. Freiser, R. Friedel, L.E. Hilliard, W.D. Johnston, Infra-red absorption spectra of metal chelates derived from 8-hydroxyquinoline, 2-methyl-8-hydroxyquinoline, and 4-methyl-8-hydroxyquinoline, Spectrochim. Acta, 8 (1956) 1–8.
[33] S. Brunauer, P.H. Emmett, E. Teller, Adsorption of gases in multimolecular layers, J. Am. Chem. Soc., 60 (1938) 309–319.
[34] B.C. Lippens, J.H. de Boer, Studies on pore systems in catalysts: V. The *t* method, J. Catal., 4 (1965) 319–323.
[35] A. Galarneau, F. Villemot, J. Rodriguez, F. Fajula, B. Coasne, Validity of the *t*-plot method to assess microporosity in hierarchical micro/mesoporous materials, Langmuir, 30 (2014) 13266–13274.
[36] E.P. Barrett, L.G. Joyner, P.P. Halenda, The determination of pore volume and area distributions in porous substances. I. Computations from nitrogen isotherms, J. Am. Chem. Soc., 73 (1951) 373–380.
[37] A.J. Bard, L.R. Faulkner, J. Leddy, C.G. Zoski, Electrochemical Methods: Fundamentals and Applications, Wiley, New York, 1980.
[38] H.-J. Butt, K. Graf, M. Kappl, Physics and Chemistry of Interfaces, John Wiley & Sons, New Jersey, 2013.
[39] M. Cabuk, M. Yavuz, H. Ibrahim Unal, Electrokinetic properties of biodegradable conducting polyaniline-graft-chitosan copolymer in aqueous and non-aqueous media, Colloids Surf., A, 460 (2014) 494–501.
[40] L. Ramenskaya, O. Kraeva, Dissociation constants for the zinc(II)-8-hydroxyquinoline complexes in aqueous and sodium dodecyl sulfate micellar solutions, Russ. J. Phys. Chem., 80 (2006) 90–94.
[41] E.F. Chaúque, L.N. Dlamini, A.A. Adelodun, C.J. Greyling, J.C. Ngila, Modification of electrospun polyacrylonitrile nanofibers with EDTA for the removal of Cd and Cr ions from water effluents, Appl. Surf. Sci., 369 (2016) 19–28.
[42] G. Bolt, W. van Riemsdijk, Physico-Chemical Models, Elsevier Scientific Publishing Company, Amsterdam, 1982.
[43] B. Vincent, B. Bijsterbosch, J. Lyklema, Competitive adsorption of ions and neutral molecules in the stern layer on silver iodide and its effect on colloid stability, J. Colloid Interface Sci., 37 (1971) 171–178.
[44] B. Ara, M. Muhammad, Rani, T. Ul Haq Zia, K. Gul, Selective removal of copper and cobalt from aqueous environment using new Cu(II) and Co(II) imprinted polymer and their determination by flame atomic absorption spectrophotometry, Desal. Water Treat., 191 (2020) 173–184.
[45] T. Wang, J. Wu, Y. Zhang, J. Liu, Z. Sui, H. Zhang, W.-Y. Chen, P. Norris, W.-P. Pan, Increasing the chlorine active sites in the micropores of biochar for improved mercury adsorption, Fuel, 229 (2018) 60–67.
[46] Y. Liu, Z. Liu, J. Gao, J. Dai, J. Han, Y. Wang, J. Xie, Y. Yan, Selective adsorption behavior of Pb(II) by mesoporous silica SBA-15-supported Pb(II)-imprinted polymer based on surface molecularly imprinting technique, J. Hazard. Mater., 186 (2011) 197–205.
[47] T.-H. Liou, Development of mesoporous structure and high adsorption capacity of biomass-based activated carbon by phosphoric acid and zinc chloride activation, Chem. Eng. J., 158 (2010) 129–142.
[48] S. Karaca, A. Gürses, M. Ejder, M. Açıkyıldız, Adsorptive removal of phosphate from aqueous solutions using raw and calcinated dolomite, J. Hazard. Mater., 128 (2006) 273–279.
[49] G.R. Belton, Langmuir adsorption, the Gibbs adsorption isotherm, and interfacial kinetics in liquid metal systems, Metall. Mater. Trans. B, 7 (1976) 35–42.
[50] T. Wirawan, G. Supriyanto, A. Soegianto, Adsorption of zinc(II) onto Zn(II)-ionic imprinted polymer, IOP Conf. Ser.: Mater. Sci. Eng., 546 (2019) 022036.
[51] M. Özdemir, Ö. Durmuş, Ö. Şahin, C. Saka, Removal of methylene blue, methyl violet, rhodamine B, alizarin red, and bromocresol green dyes from aqueous solutions on activated cotton stalks, Desal. Water Treat., 57 (2016) 18038–18048.
[52] Y. Liu, Z. Liu, Y. Wang, J. Dai, J. Gao, J. Xie, Y. Yan, A surface ion-imprinted mesoporous sorbent for separation and determination of Pb(II) ion by flame atomic absorption spectrometry, Microchim. Acta, 172 (2011) 309–317.
[53] H. Freundlich, Über die adsorption in lösungen, Z. Phys. Chem., 57 (1907) 385–470.
[54] J. Appel, Freundlich's adsorption isotherm, Surf. Sci., 39 (1973) 237–244.
[55] G. Crini, P.-M. Badot, Application of chitosan, a natural aminopolysaccharide, for dye removal from aqueous solutions by adsorption processes using batch studies: a review of recent literature, Prog. Polym. Sci., 33 (2008) 399–447.
[56] M.G.B.H. Ismail, C.N. Weng, H.A. Rahman, N.A. Zakaria, Freundlich isotherm equilibrium equastions in determining effectiveness a low cost absorbent to heavy metal removal in wastewater (leachate) at Teluk Kitang Landfill, Pengkalan Chepa, Kelantan, Malaysia, J. Geogr. Earth Sci., 1 (2013) 1–8.
[57] F. Haghseresht, G. Lu, Adsorption characteristics of phenolic compounds onto coal-reject-derived adsorbents, Energy Fuels, 12 (1998) 1100–1107.
[58] W. Zhang, Q. Li, J. Cong, B. Wei, S. Wang, Mechanism analysis of selective adsorption and specific recognition by molecularly imprinted polymers of Ginsenoside Re, Polymers, 10 (2018) 216, doi: 10.3390/polym10020216.
[59] N.D. Hutson, R.T. Yang, Theoretical basis for the Dubinin-Radushkevitch (DR) adsorption isotherm equation, Adsorption, 3 (1997) 189–195.
[60] K. Foo, B.H. Hameed, Insights into the modeling of adsorption isotherm systems, Chem. Eng. J., 156 (2010) 2–10.
[61] E.R. Monazam, L.J. Shadle, D.C. Miller, H.W. Pennline, D.J. Fauth, J.S. Hoffman, M.L. Gray, Equilibrium and kinetics analysis of carbon dioxide capture using immobilized amine on a mesoporous silica, AlChE J., 59 (2013) 923–935.
[62] I.M. Ahmed, M.S. Gasser, Adsorption study of anionic reactive dye from aqueous solution to Mg–Fe–CO_3 layered double hydroxide (LDH), Appl. Surf. Sci., 259 (2012) 650–656.
[63] A.R. Kul, N. Caliskan, Equilibrium and kinetic studies of the adsorption of Zn(II) ions onto natural and activated kaolinites, Adsorpt. Sci. Technol., 27 (2009) 85–105.
[64] F. Zhu, L. Li, J. Xing, Selective adsorption behavior of Cd(II) ion-imprinted polymers synthesized by microwave-assisted inverse emulsion polymerization: adsorption performance and mechanism, J. Hazard. Mater., 321 (2017) 103–110.
[65] A.L.P. de Araujo, M.L. Gimenes, M.A.S.D. de Barros, M.G.C. da Silva, A kinetic and equilibrium study of zinc removal by Brazilian bentonite clay, Mater. Res., 16 (2013) 128–136.
[66] X. Ao, H. Guan, Preparation of Pb(II) ion-imprinted polymers and their application in selective removal from wastewater, Adsorpt. Sci. Technol., 36 (2018) 774–787.
[67] A.E. Regazzoni, Adsorption kinetics at solid/aqueous solution interfaces: on the boundaries of the pseudo-second-order rate equation, Colloids Surf., A, 585 (2020) 124093, doi: 10.1016/j.colsurfa.2019.124093.
[68] B. Ara, M. Muhammad, M. Salman, R. Ahmad, N. Islam, T. ul Haq Zia, Preparation of microspheric Fe(III)-ion-imprinted polymer for selective solid phase extraction, Appl. Water Sci., 8 (2018) 41, doi: 10.1007/s13201-018-0680-3.
[69] J. Long, X. Luo, X. Yin, X. Wu, An ion-imprinted polymer based on the novel functional monomer for selective removal of Ni(II) from aqueous solution, J. Environ. Chem. Eng., 4 (2016) 4776–4785.
[70] B. Ara, M. Muhammad, H. Amin, Noori, R. Begum, S. Jabeen, S. Gul, T. ul Haq Zia, H. Nasir, Synthesis of ion-imprinted polymers by copolymerization of Zn(II) and Al(III)8-hydroxy quinolone complexes with divinylbenzene and methacryclic acid, Polym. Plast. Technol. Eng., 55 (2016) 1460–1473.
[71] Y.-S. Ho, G. McKay, The kinetics of sorption of divalent metal ions onto sphagnum moss peat, Water Res., 34 (2000) 735–742.
[72] Y.-S. Ho, G. McKay, Pseudo-second-order model for sorption processes, Process Biochem., 34 (1999) 451–465.

[73] Ö. Gerçel, A. Özcan, A.S. Özcan, H.F. Gercel, Preparation of activated carbon from a renewable bio-plant of *Euphorbia rigida* by H_2SO_4 activation and its adsorption behavior in aqueous solutions, Appl. Surf. Sci., 253 (2007) 4843–4852.
[74] F.-C. Wu, R.-L. Tseng, R.-S. Juang, Initial behavior of intraparticle diffusion model used in the description of adsorption kinetics, Chem. Eng. J., 153 (2009) 1–8.
[75] N. Randhawa, N. Das, R. Jana, Adsorptive remediation of Cu(II) and Cd(II) contaminated water using manganese nodule leaching residue, Desal. Water Treat., 52 (2014) 4197–4211.
[76] Z. Aly, A. Graulet, N. Scales, T. Hanley, Removal of aluminium from aqueous solutions using PAN-based adsorbents: characterisation, kinetics, equilibrium and thermodynamic studies, Environ. Sci. Pollut. Res., 21 (2014) 3972–3986.
[77] M. Doğan, H. Abak, M. Alkan, Adsorption of methylene blue onto hazelnut shell: kinetics, mechanism and activation parameters, J. Hazard. Mater., 164 (2009) 172–181.